Chirol Clementine (Orcid ID: 0000-0003-0932-4725)

Evans Ben (Orcid ID: 0000-0003-0643-526X)

Brooks Helen (Orcid ID: 0000-0002-8291-4070)

Effect of vegetation cover and sediment type on 3D subsurface structure and shear strength in saltmarshes

Authors: Clementine Chirol[1*], Kate L. Spencer[1], Simon J. Carr[2], Iris Möller[3], Ben Evans[4], Jason Lynch[5], Helen Brooks[4], Katherine R Royse[6]

[1] School of Geography, Queen Mary University of London, Mile End Road, London E1 4NS, UK

[2] University of Cumbria, Rydal Road, Ambleside LA22 9BB, UK

[3] Department of Geography, Trinity College Dublin, Museum Building, Dublin 2, Ireland

[4] Department of Geography, University of Cambridge, Downing Place, Cambridge CB2 3EN, UK

[5] Department of Geography, University College London & Zoological Society of London, Gower Street, London, WC1E 6BT, UK

[6] British Geological Survey, Nicker Hill, Keyworth, Nottingham NG12 5GG, UK

*Corresponding author current affiliation: Université de Lorraine, INRAE, LSE, F-54000 Nancy, France. Email addresses: clementine.chirol@univ-lorraine.fr; clementine.chir@hotmail.fr

Keywords: Saltmarsh; Shear Strength; X-Ray Computed Microtomography; Porosity; Root architecture

Running head: Effects of root and pore structures on saltmarsh strength

Acknowledgements

We acknowledge funding from the National Environment Research Council (NERC) for the research project RESIST(UK) (standard grant number NE/R01082X/1). We

would like to thank the School of Geography laboratory manager Michelle Day at Queen Mary University London for the use of their Nikon Metrology XT H 225 X-ray Computed Tomography (μCT) system, and laboratory instrument technician Dr Natalie Ludgate for her assistance with the sediment analysis, contribution to method development for the sodium adsorption ratio analysis and the operation of the ICP-OES.

Data Availability Statement

The dataset used in this study will be made openly available through the NERC Grants Data Management Plan at the National Geoscience Data Centre (NGDC), after a 2-year embargo period.

NERC Grant Reference No: NE/R01082X/1

Grant Title: Response of Ecologically-mediated Shallow Intertidal Shores and their Transitions to extreme hydrodynamic forcing in UK settings (RESIST-UK)

Principal Investigator: Dr Iris Möller

Conflict of Interest

The authors have no conflicts of interest to declare.

Effect of vegetation cover and sediment type on 3D subsurface structure and shear strength in saltmarshes

Keywords: Saltmarsh; Shear Strength; X-Ray Computed Microtomography; Porosity; Root architecture

Abstract

The vulnerability of saltmarshes to lateral erosion at their margin depends on the local biogeomorphological properties of the substrate. In particular, the 3D architecture of pore and root systems is expected to influence shear strength, with repercussions for the wider-scale stability of saltmarshes. We apply X-Ray Computed Microtomography (µCT) to visualise and quantify subsurface structures in two UK saltmarshes at Tillingham Farm, Essex (silt/clay rich substrate) and Warton Sands (sand rich substrate), with four types of ground cover: bare ground, *Spartina spp*, *Salicornia spp* and *Puccinellia spp*. We extracted µCT structural parameters that characterise pore and root morphologies at each station, and compared them with field measurements of shear strength using a principal component analysis and correlation tests. The 3D volumes show that species-dependent variations in root structures, plant colonisation events and bioturbation activity control the morphology of macropores, while sediment cohesivity determines the structural stability and persistence of these pore structures over time, even after the vegetation has died. Areas of high porosity and high mean pore thickness were correlated to lower values of shear strength, especially at Tillingham Farm where well-connected vertical systems of macropores were associated with current or previous colonisation by *Spartina spp*. However, while well-connected systems of macropores may lower the local deformation threshold of the sediment, they also encourage drainage, promote vegetation growth and reduce the marsh vulnerability to hydrodynamic forces. The

highest values of shear strength at both sites were found under *Puccinellia spp*, and were associated with a high density of mesh-like root structures that bind the sediment and resist deformation. Future studies of marsh stability should ideally consider time series of vegetation cover, especially in silt/clay-dominated saltmarshes, in order to consider the potential effect of preserved buried networks of macropores on water circulation, marsh functioning and cliff-face erosion.

Introduction

Saltmarshes provide key ecosystem services such as carbon storage and water purification (Barbier et al., 2011), and are important buffer habitats between the sea and the land: because of their capacity to accumulate sediment and keep pace with rising sea levels, they have the potential to contribute towards long-term, sustainable coastal defence across the world, provided that sufficient sediment input is available (Leonardi et al., 2018). However, while these habitats are efficient at dissipating wave action during marsh surface inundation (Möller et al., 2014), they have been shown to be vulnerable to lateral erosion at the margin (Bendoni et al., 2016). It has been argued that the destruction and rejuvenation of saltmarshes is a natural process occurring over an order of a few hundred or thousand years, dominated by sedimentological processes (Van de Koppel et al., 2005; Chauhan, 2009; Fagherazzi, 2013). However, in the context of anthropological pressure on coastal environments, sediment starvation, and increased wave impact and storm frequency accompanying sea-level rise, trends of net saltmarsh loss have been observed around the world (Allen, 2000; Schwimmer, 2001; Gedan et al., 2009; Gu et al., 2018). While wind-waves play a primary role on long-term marsh edge erosion at the landscape scale, local marsh characteristics such as vegetation cover are also important (Finotello et al., 2020). Therefore rates of saltmarsh erosion from wave

action are variable from marsh to marsh (Ford et al., 2016; Wang et al., 2017), and even over small spatial scales within the same marsh (Van de Koppel et al., 2005; Priestas et al., 2015; Wang et al., 2017; Bernik et al., 2018). Since local vulnerabilities in the marsh structure can have broader implications for the whole marsh and lead to widespread erosion (Leonardi and Fagherazzi, 2015; Bendoni et al., 2016), better understanding of what causes these local changes in stability or susceptibility to erosion is needed to more accurately project potential future losses and efficiently mitigate against these in the context of a changing climate.

The intrinsic capacity of saltmarsh substrates to resist hydrodynamic erosive forces at the local scale is often measured as localised shear strength. While wave flume experiments can help us understand the specific effect of wave thrust on the erosion of 'transposed' marsh cliffs, *in situ* measurements have the advantage of preventing disturbance during sampling, transport and storage (Grabowski, 2014). At the local scale, this resistance to deformation depends on bulk sediment properties such as the grain size, cohesivity and water retention properties of the sediment (Crooks and Pye, 2000; Grabowski et al., 2011), but also on biogeomorphological factors such as the presence and morphology of vegetation, roots and pores (Wang et al., 2017; Brooks et al., 2020). While influences on surface shear strength, such as the presence of vegetation and biofilm, have been extensively studied (Feagin et al., 2009; Gedan et al., 2011), the impacts of subsurface structures and processes on shear strength remain challenging to observe and quantify (Brooks et al., 2020). Structural pores or macropores, caused by cracks, burrows and decaying roots (as opposed to micropores or matrix pores which are formed by the space between sediment particles (Rabot et al., 2018)), can create areas of structural vulnerability in the soil (Vu et al., 2017). They can also promote vertical water movement in the

subsurface environment, improve drainage (Tempest et al., 2015) and facilitate root growth (Li et al., 2005). Roots are another important architectural component of the marsh substrate. The tensile strength provided by the roots complements the sediment, which is naturally strong in compression (Gyssels et al., 2005), and thus helps to prevent block failure (Wang et al., 2017; Brooks et al., 2020). However, the roots' exact role on substrate stability depends on species- and environment-specific structural characteristics (Gyssels et al., 2005). A particularly understudied aspect is how the 3D architectures of roots and pore networks interact within different types of substrates, and influence the internal shear strength of a saltmarsh (Brooks et al., 2020).

X-Ray Computed Microtomography (µCT) combines the penetrating capacity of X-Rays with 3D-volume reconstruction to observe the internal 3D structure of objects in a non-destructive manner (Cnudde and Boone, 2013). µCT has been applied extensively to agricultural soils to investigate the impact of subsurface structures on crucial soil functions such as water infiltration (Katuwal et al., 2015; Tracy et al., 2015; Jarvis et al., 2017; Müller et al., 2018; Pot et al., 2020), root-pore interactions and patterns of plant growth (Lucas et al., 2019; Hu et al., 2020; Pulido-Moncada et al., 2020). In recent years, the technique has been extended to saltmarsh substrates (Spencer et al., 2017; Dale et al., 2019; Van Putte et al., 2019); however, distinguishing roots from pores is challenging because their greyscale values overlap due to the partial volume effect (Cnudde and Boone, 2013; Helliwell et al., 2013), especially in these complex heterogenous substrates. Indeed saltmarshes are transitional habitats formed by a constant interplay of sediment deposition and erosional processes, and where ground cover and other soil characteristics can vary rapidly both in space and time. Episodes of storm surges, colonisation by burrowing

organisms, or colonisation and die-off of plants, may be recorded as sedimentary features, and therefore sub-surface features may be critical to interpreting surface information and marsh response. Recent studies have developed new approaches for root analysis (Author's own, 2021) which allow us to capture the complexity of heterogeneous saltmarsh substrates with unprecedented precision.

This study applies X-ray Computed Microtomography to the 3D structural analysis of roots and pores in two UK saltmarshes of contrasting sediment type and under four contrasting ground covers (bare ground, *Spartina spp*, *Salicornia spp*, *Puccinellia spp*). We provide a detailed analysis, both visual and quantitative, of saltmarsh belowground structures, and discuss the interplay of root and pore systems under different ground covers and sediment types. We select parameters that best capture the structural variability of roots and pores, and explore correlations between substrate morphology and internal shear strength using a principal component analysis. Taking into consideration other geochemical factors of erodibility such as the proportion of clay sized particles, the organic matter content and the dispersibility of the clay, we then discuss the wider implications in terms of how sediment properties and morphology contribute to marsh stability at different spatial scales, and provide recommendations for further studies.

Methods

We analysed belowground structure and shear strength at two minerogenic saltmarshes in the UK. In order to compare the effect of vegetation and substrate on the sub-surface structure, we considered two sediment types (sand-rich at Warton Sands and silt/clay-rich at Tillingham) and four types of ground cover (bare ground, *Spartina spp*, *Salicornia spp*, *Puccinellia spp*), for a total of eight stations (Figure 1). The ground cover choices reflect the zonation of vegetation in the saltmarshes, with

bare ground mudflats fronting the marsh, then pioneer species *Spartina spp* and *Salicornia spp*, and lower marsh species *Puccinellia spp* (Figure 2). This may inform us on how a saltmarsh inherits structural features as it accretes vertically from fronting mudflat to an inner marsh. The plant species were also chosen for their contrasting root structures: *Spartina spp* have long stems with internal voids as an adaptation strategy to anoxic conditions (Mitsch and Gosselink, 1986); *Salicornia spp* have a shallow and sparse root system and *Puccinellia spp* have a dense system of thin roots (Chapman, 1960).

Three replicate sediment cores (15 cm depth and 15 cm diameter) were collected at each station in January 2019. The replicates were spaced within 0.5 - 2 m from one another to ensure that all replicates are independent but have similar substrates. The sediment cores were collected to minimise disturbance of structural features, as summarised in Carr *et al.* (2020). After extraction, the cores were stored upright in a cooling box filled with bubble wrap to minimise disturbance during transport, and stored at 4 ^{o}C until required.

The whole, intact cores were scanned using a Nikon Metrology XT H 225 X-ray Computed Microtomography (µCT) system at 205 kV and 46 µA (9.4 W). The exposure time was 500 ms at 36 dB gain. A Cu 1 mm copper filter was used to reduce beam hardening artefacts. 4486 projections were acquired with four frames per projection, for a scan time of 4.5 hours. The effective voxel size is 61.79 µm, downscaled to 62.5 µm during volume reconstruction. The scanned volumes were cropped to a 8.75*8.75 cm square base to reduce edge effects and remove any disturbance from sampling. All 24 scanned volumes were processed following the method detailed in Author's own (2021) to segment the µCT data into three phases: pore space, organic matter elements (including roots and degraded organic matter)

and finally the bulk inorganic mineral phase. All elements larger than 5,000 voxels (1.22 mm^3) were removed as noise, and the minimal thickness of elements at any point is twice the resolution, so 125 µm. This method was developed to distinguish live and decayed (necromass) roots from pores in heterogeneous saltmarsh soils, which makes it highly relevant here.

Each phase was visualised in 3D using the volume rendering software Drishti (Limaye, 2012), and a detailed morphological analysis was performed using the automated software plugin “Particle Analysis” for ImageJ (Schindelin et al., 2012) to extract a number of shape parameters (Table 1). Out of these parameters we selected those that best represent the structural differences between vegetation and sediment types, basing ourselves on previous studies (Spencer et al., 2017; Rabot et al., 2018) and on our own observation of the dataset. Each selected variable was then normalised within the interval [0 1] to visualise variations across stations for all variables, and plotted as spider plots.

While the main focus of the paper is to establish relationships between substrate structure and shear strength, other parameters commonly associated with soil stability or vulnerability to erosion were also considered. These include the proportion of clay sized particles, which influences the cohesivity of the sediment, the proportion of organic matter as determined by loss on ignition, and the sodium adsorption ratio of the sediment. The latter considers how high content of exchangeable Na+ in the soil can lead to the formation of thick water films around the clay particles and to slow rates of sediment consolidation, thus making the marsh more prone to erosion (Crooks and Pye, 2000). Three replicate cores per station were taken for the analysis of the sodium adsorption ratio at two depths (0-1 cm and 7-8 cm from the surface): samples were freeze-dried, sieved at 2 mm, then mixed

with a recorded mass of distilled water until the obtention of a saturation paste as outlined by Rowell (1994), and left overnight for the cations to equilibrate. The samples were then centrifuged to retrieve the extracts, and the exchanged cations were measured in the extract using inductively coupled plasma optical emission spectrometry (ICP-OES). The sodium adsorption ratio was then calculated as SAR = $[Na+] /([Ca^{2+}] + [Mg^{2+}])^{0.5}$ with [ ] the concentration in $mmol^{-1}$. Of the three replicate cores, one core per station was also processed for particle size analysis by laser granulometry and organic matter content every 1-2cm from the surface to 15cm deep (see Table 2 for details). Measurements of organic matter content, including both particulate organic carbon and roots were obtained by loss on ignition following the method by Rowell et al. (1994): soil samples were first air-dried, heated overnight at 105° C, and then weighed and combusted at 500 °C overnight.

Finally, shear vane data were collected in August and September 2019 from a distributed survey across a large area of the Tillingham Farm and Warton Sands saltmarshes. The shear vane measures pressure applied at failure point at a depth of 7.5 cm from the surface by rotating a handle against the vane head, and quantifies the undrained geotechnical shear strength of the sediment, that is to say its resistance to deformation and fracture at a very local scale (Grabowski, 2014). While there is a spatial and temporal mismatch between the shear strength measurements and the position of our sediment cores, the survey was designed to capture the characteristic shear strength for each station, with measurements taken at a frequency of 150 per sediment and vegetation type. A summary of the sampling procedure for each data type is provided in Table 2.

Due to the small number of measurements for all considered parameters except the shear strength, the normality hypothesis cannot be assumed to distinguish between

groups using ANOVA tests. We used the non- parametric tests Kolmogorov-Smirnov for normality and Bartlett and Levene for homoscedasticity. When the conditions of normal distribution and homogeneous variances were not met, we relied on the non-parametric test Kruskal-Wallis, which is less sensitive to outliers.

Finally, we performed a Principal Component Analysis (PCA) to compare the µCT morphological characteristics to the shear strength in order to estimate which structural parameters are the main drivers of variability between locations. Since we want to focus on the role of soil structure on shear strength, sedimentological and geochemical properties were not included in the PCA; instead, their specific contributions to shear strength were studied using linear regression. PCA transforms the variables in a dataset into a set of principal components in order to reduce the dimensionality while retaining as much of the variation as possible (Jolliffe, 2002). PCA assumes that all considered variables follow a normal distribution, and that the variables considered fully represent the statistical variation in the dataset: however, even if these conditions are not met, as is the case in our dataset according to the Kolmogorov-Smirnov test, PCA is a robust analytical tool that still provides a useful means to group intercorrelated parameters in function of their contribution to the overall variability of the dataset (Steel, 1996; Jolliffe, 2002; Reid and Spencer, 2009; Chirol et al., 2018). It is therefore well suited to the analysis of novel parameters such as µCT structural indicators, because their relations with one another and with shear strength are still poorly understood. For this step, we subsampled the shear strength dataset to 3-4 data points per location while remaining representative of the mean and spread of the sample. We calculated the 10th, 50th and 90th percentiles for all stations with three replicates, and 10th, 40th, 60th and 90th percentiles for the station TF PUC where four replicates had been selected. All percentiles were sorted

randomly to not skew the dataset. All datasets presented in the paper can be found as Supplementary Information.

Results

Subsurface structural properties

The 3D volumes highlight the complexity of pore and root networks under the surface of a saltmarsh (Figure 3, Appendix 1): the main structures observed at each station are summarised in Table 3. Three main types of macropores are observed in our samples: (1) highly connected vertical pore systems, (2) sub-horizontal sheets of porosity corresponding to internal cracks (the internal cracks observed during sampling were surrounded by iron precipitates, confirming them as pre-existing structures rather than a product of disturbance during core sampling), and (3) disconnected pores ordered along a horizontal plane, corresponding to bioturbation horizons. We find a highly connected network of macropores with a vertical orientation at Tillingham Farm at the bare ground, *Salicornia spp* and *Spartina spp* stations, and a sparser network at Warton Sands under the *Spartina spp* station. Internal cracks in the cores with a more horizontal orientation are found under *Puccinellia spp* at both Warton Sands and Tillingham Farm. Finally, bioturbation horizons with characteristic straight or looping burrows are found at Warton Sands under the bare ground and *Salicornia spp* stations. Large round porosity elements are also found under the *Spartina spp* station at Tillingham Farm, corresponding to empty shells found in the field.

The organic matter elements detected by µCT belong either to disconnected fragments corresponding to the necromass or to a live root system. Necromass is detected under all stations at both Warton Sands and Tillingham Farm, but is particularly conspicuous at the bare ground stations where live root systems are

absent. In the vegetated cores, the organic phase is dominated by the live root system. While root system architecture is challenging to visualise in the more diverse Tillingham cores, key differences between the root systems of the three vegetation types can be distinguished at Warton Sands. *Puccinellia spp* plants have a highly fibrous root system while *Salicornia spp* and *Spartina spp* are closer to a tap root morphology according to the classification system by Delory et al. (2018). The tap root belonging to *Salicornia spp* is shorter, thinner and shallower than that of *Spartina spp*. Other classification systems distinguish herringbone from dichotomous root patterns based on their branching configuration (Lupini et al., 2018); however, the complexity of the root networks and the proximity of the roots to one another make them appear interconnected in µCT, which masks the exact branching pattern and makes it difficult to resolve the different networks.

Tables 4 and 5 show the mean morphological parameters that characterise the pore and root systems at each station. The pore fraction is systematically higher at Tillingham Farm (4-8 %) than at Warton Sands (1-3 %). The mean distance between pores is lower (1-3 mm versus 3-15 mm) and the pore systems are better connected (46-73 % versus 4-51 %). Furthermore, the spider plots show structural differences between pore systems that look similar in the 3D volumes, such as those found under the bare ground, *Salicornia spp* and *Spartina spp* stations at Tillingham Farm: the pores under *Spartina spp* and under the bare ground station are thicker than under *Salicornia spp*, while the *Spartina spp* station has the smallest number of pores due to having the best connectivity, and has the highest complexity according to the Euler-Poincaré characteristic (~17,000, see Figure 4). The porosity at the Warton Sands stations has a lower structural complexity than at Tillingham Farm, except under *Spartina spp*, where the pore complexity is similar to that of the *Spartina spp* station at Tillingham Farm. The bare ground stations have contrasting pore structures: at Tillingham Farm, the bare ground station has the most and the thickest macropores, while at Warton Sands, the bare ground has the lowest fraction of macropores. Out of the vegetation covers considered, the *Puccinellia spp* stations have the fewest macropores at both Warton Sands and Tillingham Farm. The *Salicornia spp* and *Spartina spp* stations have similar fractions of macropores, but the macropores at the *Spartina spp* stations have a higher level of internal complexity.

The morphological characteristics of the root systems under the *Spartina spp*, *Salicornia spp* and *Puccinellia spp* stations depend more on vegetation species than on sediment type (Figure 5). The ground cover types can be ordered according to their organic fraction and number of connected organic matter elements respectively,

from lowest to highest: bare ground (<0.2 %, 200-700), *Salicornia spp* (0.4-1 %, 800-2500), *Spartina spp* (2-3 %, 1600-1900) and *Puccinellia spp* (2-3 %, 3500-3600). The root systems can also be ordered according to their connectivity and complexity, again, from lowest to highest: bare ground (5-28 %, 200-300), *Salicornia spp* (20-21 %, 3000-4000), *Puccinellia spp* (24-32 %, 10000-24000) and *Spartina spp* (65-73 %, 26000-32000). The mean distance between organic matter elements is within the range 1-2 mm for most vegetation types except *Salicornia spp* at Warton Sands (5 mm); predictably, this mean distance is greater in the bare ground stations (4-17 mm).

Geotechnical, sedimentological and geochemical properties

Since the conditions of normal distribution and homogeneous variances are not met for the geotechnical, sedimentological and geochemical properties considered (see Appendix Table 1), we rely instead on visual observation and on the Kruskal-Wallis test to interpret differences between the locations; the p-values for these tests are shown in Table 7. Based on a visual observation of the boxplots, compared to Warton Sands, core samples collected from Tillingham Farm have a higher proportion of clay-sized particles (84-96 % versus 44-58 %) and of organic matter content (6-15 % versus 2-3 %), for all vegetation types (Table 6, Figure 6A-6B). According to Kruskal-Wallis, TF BG and WS BG have statistically different median clay fractions, and the median organic matter concentration is significantly different between Tillingham Farm and Warton Sands, except for TF BG, which is not significantly different from WS SAL and WS SPA. The difference in organic matter concentration between Warton Sands and Tillingham Farm is more pronounced at the *Puccinellia spp* stations. This confirms that the two saltmarshes considered in this study are characterised by contrasting sediment types. The Tillingham Farm

samples also have a statistically higher sodium adsorption ratio (SAR) according to Kruskal-Wallis compared to those from Warton Sands (46-59 versus 21-30, Table 6, Figure 6D), with a few exceptions, such as WS SPA and TF SAL not being statistically different from either group, and TF PUC not being significantly different from WS BG. .

Greater mean values of shear strength, as well as a higher spread in the measurements, are found at Warton Sands. Out of the vegetation covers considered, the *Puccinellia spp* plots have the greatest measured shear strength (Figure 6D). According to both Kruskal-Wallis results and ANOVA tests and p-values, no statistical difference is found between the shear strength at TF BG, TF SAL and TF SPA. TF PUC has significantly higher shear strength values than the other ground covers at Tillingham Farm, but not significantly different from WS BG. All Warton Sand ground covers are significantly different from one another and are ordered as follows in order of ascending shear strength: WS BG, WS SPA, WS SAL, WS PUC. Across all ground covers and sediment types, shear strength is negatively linearly correlated with SAR ($R=-0.83$, $p=0.01$) and has a non-significant correlation with the clay fraction ($R=-0.67$, $p=0.07$). There is a very strong positive correlation between SAR and the clay fraction ($R=0.86$, $p=0.01$). No significant correlation is found between shear strength and organic matter content across the whole dataset ($R=-0.59$, $p=0.12$), but a significant positive correlation exists between the two variables at Tillingham Farm (Appendix 2). Interestingly, no significant correlation is found between organic matter content from loss on ignition and the organic fraction obtained from the µCT data ($R=0.39$, $p=0.34$), probably because loss on ignition includes particulate organic matter, and not just the live root system and the necromass.

Correlations between subsurface morphological properties and erosion resistance

We conduct a PCA to explore the controls on variability in shear strength and in the morphological characteristics of the organic matter elements and macropores under each ground cover and sediment type. The Kaiser-Meyer-Olkin (KMO) test yields a measure of sampling adequacy of 0.63, which corresponds to an acceptable but mediocre degree of common variance class. The low KMO reflects the small sample size available for the PCA (3-4 cores per ground cover type, 25 data points in total). Another limitation of PCA is the assumption that the variables selected fully represent the statistical variation of the dataset (Jolliffe, 2002), which is unlikely in a complex saltmarsh substrate. Therefore the interpretations should be treated with caution, but graphical observation of the Principal Components (PC) using biplots offers an indication of the relative importance of each considered variable (Figure 7). In order to increase the interpretability of the principal component loadings, we use a varimax rotation to rotate the orthogonal axis so that it aligns with the data points in a way that maximises the degree of variance in the data (Steel, 1996). Following varimax rotation, the first 3 PCs explain over 73% of the total variation. At each PC the variables are considered important determinants of the variability in the dataset if their loadings exceed ±0.40 (Williams et al., 2010), and shaded red in Table 8.

PC1 opposes the pore and organics emptiness with the number of pore particles: the presence/absence of vegetation is the most significant distinguisher between the cores, with the Warton Sands samples typically having fewer pores and roots than the more structurally complex core samples at Tillingham Farm, and WS BG far apart from all the other locations.

PC2 opposes shear strength and the number of organic matter elements with pore thickness and pore fraction. The clearest correlation is the negative correlation between pore thickness and shear strength. PC2 opposes WS PUC and TF BG as end members.

PC3 is dominated by variables of organic matter elements abundance and complexity (organic fraction, connectivity and Euler complexity) and by the Euler complexity of the pores. This highlights the structural differences between the *Spartina spp* cores and the bare ground cores at both Warton Sands and Tillingham Farm. *Spartina spp* have large stems and roots with a complex internal structure and internal voids, which is shown in the parameters by a more connected root system, and a higher Euler complexity of both pores and organic matter elements.

Discussion

Influence of vegetation, bioturbation and sediment cohesivity on the formation and structural stability of macropores

Compared with previous studies, the development of a novel segmentation technique combining local adaptive thresholding and tubular shape detection gives us greater confidence in our capacity to capture the complexity of a saltmarsh subsurface environment: ground referencing tests confirmed that the µCT data accurately capture regions of dense roots as well as the position and structures of macropores (Author's own, 2021). Using µCT morphological data under various types of ground cover and under different sediment types allows us to explore the potential role of subsurface structure on shear strength with an unprecedented perspective on the 3D structure and interplay of pores and roots.

One notable observation is how rare it is to find buried roots in unvegetated regions of the marsh: only small fragments of organic matter are found under the bare ground stations at Tillingham Farm and Warton Sands. However, at Tillingham Farm, macropores are found in the shape of *Spartina spp* roots, possibly from a previous episode of colonisation and die-off. The persistence of the pores even after the roots have fully decayed suggests that the above-ground plant breakage and removal occurred without causing widespread erosion of the bed or infill of the macropores, which signifies that the substrate around the pores has enough internal cohesion to retain its shape even under tidal inundation. Since no such pore system is found under the Warton Sands stations, it is probable that these complex, highly connected and vertical pore systems are less structurally stable in sandier, less-cohesive sediment types. This would explain why the distance between pores dominates the morphological differences between the Warton Sands and Tillingham Farm samples according to the first principal component of the PCA. We do find evidence of pore structures being preserved at Warton Sands, but these are thin, horizontal bioturbation horizons, with characteristic I- and U-shaped burrow structures observable in 3D (Figure 3). Burrowing organisms tend to consolidate their burrow structures by coating the walls with secretions (Kristensen and Kostka, 2005; Pagenkemper et al., 2015), which might explain why these horizons have been so well preserved.

Among the vegetated cores, *Spartina spp* and *Puccinellia spp* cores have similar volumes of organic matter elements, but very distinct root morphologies. *Spartina spp* stems have a greater connectivity and internal complexity due to their internal air spaces, giving them a perforated shaft structure, while *Puccinellia spp* root systems are detected as a fragmented mesh structure. The complexity and connectivity of the

Puccinellia spp root structure is likely to be underestimated due to fine roots falling below the detection threshold of µCT, while tap root morphologies like those of *Spartina spp* or *Salicornia spp* have reduced branching and fewer lateral roots (Vannoppen et al., 2015), making them easier to detect in µCT than fibrous morphologies. Vegetation type also has an impact on the morphology of macropores: at both Warton Sands and Tillingham Farm, we find vertically-oriented tubular pores under the *Spartina spp* stations due to the aerenchyma, and horizontally-oriented internal cracks in the sediment under the *Puccinellia spp* stations. The *Puccinellia spp* stations have a smaller volume of macropores overall, in accordance with previous observations on fibrous root systems (Vannoppen et al., 2015). The second principal component also shows correlations between the complexity of the root system and the complexity and connectivity of the pore system. These observations indicate that vegetation cover (and burrowing organisms) control the type of macropores that form within the substrate, and that the sediment type controls how well these macropores will be preserved.

Influence of substrate internal structure and geochemistry on shear strength

Higher values of shear strength are found at Warton Sands compared to Tillingham Farm, even though the sandier sediment at Warton Sands is more erosion-prone according to previous remote sensing and flume experiments (Pringle, 1995; Ford et al., 2016). This discrepancy is explained by the very localised properties measured by the shear vane, arguably at the sub-root-layer scale: while still cohesive, the higher sand content of the Warton Sand sediment might make it less deformable by the shear vane blades than the more clay-rich sediment of Tillingham Farm. The shear strength is also significantly negatively correlated to pore fraction and mean

pore thickness: large macropores offer no resistance to the shear vane, which would explain the low shear strength values recorded at TF BG compared to WS BG, even though the cohesive clay is in fact more resistant to hydrodynamic forces– as is evidenced by the persistence of the below ground *Spartina*-root-like pore structures under the bare ground cover at Tillingham Farm. The exact role of macropores on marsh stability is difficult to parse out: while previous studies have associated porosity with greater erodibility in tidal flats (Wiberg et al., 2012), vertical connected systems of macropores promote drainage, which not only reduces the water's erosive capacity at the surface (Tempest et al., 2015), but also improves sediment aeration, biogeochemical cycling, plant growth and the overall productivity of the saltmarsh (Xin et al., 2009). Therefore the instantaneous, localised weakening effect of macropores may be compensated by their indirect contribution to marsh stability. Our results highlight complex interactions between substrate structure, potential water flow and erosion vulnerability, which occur at different spatial and temporal scales. The 3D volumes of pore systems obtainable in µCT could provide a framework for water infiltration models in different types of saltmarsh substrates, and help us understand these feedback processes in future studies.

Links between shear strength and root system morphology are harder to decipher in the PCA. According to Brooks et al. (2020), in the upper 15 cm of the marsh, resistance to erosion should be controlled by both the root mat and the sediment properties. Because the binding action of fine root meshes are considered to have an impact on shear strength as measured by the shear vanes (Grabowski, 2014), we hypothesised that either the Euler-Poincaré characteristic or the mean distance to root elements could be used as a descriptor of the 3D mesh-like structure and to quantify this structure's contribution to marsh strength. Here, however, only the

number of organic matter elements is grouped with the shear strength in the second principal component's loadings. At present, while our method allows us to visualise this mesh-like structure in the 3D volumes, the resolution limit of µCT means that this mesh is too disconnected to be correctly described with quantitative parameters. The *Puccinellia spp* stations are characterised by both the highest number of root elements (Figure 5) and by the highest shear strength for both Warton Sands and Tillingham Farm (Figure 6), indicating that the mesh-like root structure does have an impact on bed/soil stability. The impact of vegetation type on shear strength appears greater in the sand-rich than in the silt/clay-rich substrate, in accordance with previous studies (Ford et al., 2016; De Battisti et al., 2019). This could be due to a facilitated root penetration in coarser sediments, which exacerbates the structural differences between tap root and mesh root traits: the observed effects of sediment type and root morphology on macropore fraction and shear strength are schematised in Figure 8. The lack of a significant relationship between shear strength and organic matter content from loss on ignition also suggests that the binding action of roots has more impact on shear strength than their contribution to organic matter content in the substrate, at least within the root zone.

Finally, we found higher sodium adsorption ratio (SAR) values at Tillingham Farm compared to Warton Sands, despite higher SAR normally being associated with a more erosion-prone sediment. This occurs because the difference in soil properties between the two sites affects the relationships between geotechnical and sedimentological properties (Appendix 2): since Warton Sands is not clay-dominated (<60 % clay), the dispersibility of the clay material present is unlikely to significantly affect the overall erodibility of the sediment. The 0.88 correlation between SAR and shear strength reported across the whole dataset is probably not, therefore, a

function of SAR but of the other factors that co-vary with SAR between the two sites and have a greater impact on shear strength. At Tillingham Farm, both the shear strength and SAR values are within the range obtained by Crooks and Pye (2000) for active saltmarshes in Essex with low proportions of calcium carbonates (SAR = 53.4-66.9; shear strength = 10.5 – 27.8 kPa). Within this clay-rich site, SAR values are more likely to have an impact on erodibility; however we see no significant differences in SAR values between the locations, which suggests that there is minimal mineralogical variation at this spatial scale and that vegetation and pore structures are a greater determinant of variations in erodibility.

Future perspectives

µCT has the potential to capture the whole 3D structural complexity of the saltmarsh: future studies could also incorporate shell deposits, or could refine the method for smaller scales to resolve fine roots. Whilst we focused on monospecific locations to describe the root structure of common saltmarsh species, the impact of species richness should also be explored: root structure depends not only on the growth strategy specific to each plant species, but can also change as a function of nutrient availability, redox potential and competition with other species (Bouma et al., 2001; Bardgett et al., 2014; De Battisti et al., 2019). Enhanced biodiversity has been found to exacerbate competition strategies between species and lead to greater root biomass and greater sediment cohesivity (Ford et al., 2016).

In order to better correlate these structures to marsh stability in future studies, further geotechnical tests and flume experiments are required to better understand the effect of different ground covers on substrate resistance to deformation and to hydrodynamic forcing, so that we may capture the different processes that contribute to marsh resistance at different scales. Indeed, the effect of local, cm-scale pore and

root structures on erosion resistance depends not only on shear strength, but also on the position and orientation of these features relatively to the dominant wind direction, water depth and tidal regime (Schwimmer, 2001; Brooks et al., 2020).

Consideration of the marsh topography and foreshore morphology will therefore be necessary to fully understand saltmarsh morphodynamics at the landscape scale. To that end, remote sensing data are frequently used to map vegetation distribution and erosion patterns (Van der Wal et al., 2008). This paper will assist in the interpretation of vegetation maps in terms of what dominant structures might be found belowground, and their effects on marsh strength. Our results also suggest that vegetation maps should ideally consider time series of vegetation covers over the years, since porosity structures inherited from certain vegetation types can be preserved underground even after the vegetation has died, at least in cohesive sediments. These buried and preserved pore networks might lower hydrodynamic forcing at the surface by facilitating water infiltration and drainage, but might also contribute to cliff-face erosion by providing areas of structural weakness.

Conclusion

In this study, we compared morphological parameters of macroporosity and root structure from X-ray Computed Microtomography with shear strength data obtained in the field in saltmarshes of contrasting sediment types and in four contrasting ground cover types, in order to explore links between marsh subsurface structure and marsh strength. Our results show that a combination of ecological factors (different root structures create different porosity elements) and sedimentological factors (the soil cohesivity controls its capacity to preserve these pore structures even after the above-ground vegetation has died) play a significant role in determining the macropore structures in saltmarshes. Large vertically-connected

systems of macropores were found at Tillingham Farm under all ground covers except *Puccinellia spp*: these macropores reduce the internal shear strength, but may facilitate water infiltration and drainage and reduce erosive forces at the surface. The mesh-like root structure characteristic of *Puccinellia spp* contrasts with the tap root morphology at *Salicornia spp* and *Spartina spp*, and was found to be the most efficient at increasing the shear strength due to its binding action, at least when looking at mono-specific locations. At the scale considered, vegetation type was a better predictor of shear strength than sodium adsorption ratio, which did not change significantly from location to location at Tillingham Farm. The subsurface structure and strength of saltmarshes results from a complex balance between the marsh history (succession of ground covers and species over time, storm events and other variations in sedimentation rates leading to different sedimentary horizons) and the capacity of the marsh substrate to preserve its internal structure, which depends on the cohesivity of the sediment but also on consolidation by living organisms and plants.

References

Allen J. 2000. Morphodynamics of Holocene salt marshes: a review sketch from the Atlantic and Southern North Sea coasts of Europe. Quaternary Science Reviews **19** : 1155–1231. DOI: 10.1016/S0277-3791(99)00034-7 [online] Available from: http://linkinghub.elsevier.com/retrieve/pii/S0277379199000347

Barbier EB, Hacker SD, Kennedy C, Kock EW, Stier AC, Silliman BR. 2011. The value of estuarine and coastal ecosystem services. Ecological Monographs **81** : 169–193. DOI: 10.1890/10-1510.1

Bardgett RD, Mommer L, Vries FT De. 2014. Going underground : root traits as

drivers of ecosystem processes. Trends in Ecology & Evolution **29** : 692–699. DOI: 10.1016/j.tree.2014.10.006 [online] Available from: http://dx.doi.org/10.1016/j.tree.2014.10.006

De Battisti D, Fowler MS, Jenkins SR, Skov MW, Rossi M, Bouma TJ, Neyland PJ, Griffin JN. 2019. Intraspecific Root Trait Variability Along Environmental Gradients Affects Salt Marsh Resistance to Lateral Erosion. Frontiers in Ecology and Evolution **7** : 1–11. DOI: 10.3389/fevo.2019.00150

Bendoni M, Mel R, Solari L, Francalanci S, Oumeraci H. 2016. Insights into lateral marsh retreat mechanism through localized field measurements. Water Resources Research **52** : 1446–1464. DOI: 10.1111/j.1752-1688.1969.tb04897.x

Bernik BM, Eppinga MB, Kolker AS, Blum MJ. 2018. Clonal Vegetation Patterns Mediate Shoreline Erosion. Geophysical Research Letters **45** : 6476–6484. DOI: 10.1029/2018GL077537

Bouma TJ, Nielsen KL, Van Hal J, Koutstaal B. 2001. Root system topology and diameter distribution of species. Functional Ecology **15** : 360–369.

Brooks H, Möller I, Carr S, Chirol C, Christie E, Evans B, Spencer KL, Spencer T, Royse K. 2020. Resistance of salt marsh substrates to near-instantaneous hydrodynamic forcing. Earth Surface Processes and Landforms DOI: 10.1002/esp.4912

Carr SJ, Diggens LM, Spencer KL. 2020. There is no such thing as 'undisturbed' soil and sediment sampling: sampler-induced deformation of salt marsh sediments revealed by 3D X-ray computed tomography. Journal of Soils and Sediments **20** : 2960–2976. DOI: 10.1007/s11368-020-02655-7

Chapman VJ. 1960. Salt marshes and salt deserts of the world

Chauhan PPS. 2009. Autocyclic erosion in tidal marshes. Geomorphology **110** : 45–57. DOI: 10.1016/j.geomorph.2009.03.016 [online] Available from: http://dx.doi.org/10.1016/j.geomorph.2009.03.016

Author's own, 2021. Pore, live root and necromass quantification in complex heterogeneous wetland soils using X-ray computed tomography. Geoderma **387** : 114898. DOI: 10.1016/j.geoderma.2020.114898 [online] Available from: https://doi.org/10.1016/j.geoderma.2020.114898

Chirol C, Haigh ID, Pontee N, Thompson CE, Gallop SL. 2018. Parametrizing tidal creek morphology in mature saltmarshes using semi-automated extraction from lidar. Remote Sensing of Environment **209** : 291–311. DOI: 10.1016/j.rse.2017.11.012

Cnudde V, Boone MN. 2013. High-resolution X-ray computed tomography in geosciences: A review of the current technology and applications. Earth-Science Reviews **123** : 1–17. DOI: 10.1016/j.earscirev.2013.04.003 [online] Available from: http://dx.doi.org/10.1016/j.earscirev.2013.04.003

Crooks S, Pye K. 2000. Sedimentological controls on the erosion and morphology of saltmarshes: implications for flood defence and habitat recreation. Geological Society, London, Special Publications **175** : 207–222. DOI: 10.1144/GSL.SP.2000.175.01.16 [online] Available from: http://sp.lyellcollection.org/cgi/doi/10.1144/GSL.SP.2000.175.01.16 (Accessed 27 November 2014)

Dale J, Cundy AB, Spencer KL, Carr SJ, Croudace IW, Burgess HM, Nash DJ. 2019. Sediment structure and physicochemical changes following tidal inundation at a large open coast managed realignment site. Science of the Total Environment **660** :

1419–1432. DOI: 10.1016/j.scitotenv.2018.12.323 [online] Available from: https://doi.org/10.1016/j.scitotenv.2018.12.323

Delory BM, Li M, Topp CN, Lobet G. 2018. archiDART v3.0: A new data analysis pipeline allowing the topological analysis of plant root systems. F1000Research **7** : 1–14. DOI: 10.12688/f1000research.13541.1

Fagherazzi S. 2013. The ephemeral life of a salt marsh. Geology **21** : 943–944. DOI: 10.1130/0091-7613

Feagin RA, Lozada-Bernard SM, Ravens TM, Möller I, Yeager KM, Baird AH. 2009. Does vegetation prevent wave erosion of salt marsh edges? Proceedings of the National Academy of Sciences of the United States of America **106** : 10109–13. DOI: 10.1073/pnas.0901297106 [online] Available from: http://www.pnas.org/cgi/content/long/106/25/10109 (Accessed 10 January 2015)

Finotello A, Marani M, Carniello L, Pivato M, Roner M, Tommasini L, D'alpaos A. 2020. Control of wind-wave power on morphological shape of salt marsh margins. Water Science and Engineering **13** : 45–56. DOI: 10.1016/j.wse.2020.03.006 [online] Available from: https://doi.org/10.1016/j.wse.2020.03.006

Ford H, Garbutt A, Ladd C, Malarkey J, Skov MW. 2016. Soil stabilization linked to plant diversity and environmental context in coastal wetlands. Journal of Vegetation Science **27** : 259–268. DOI: 10.1111/jvs.12367

Gedan KB, Kirwan ML, Wolanski E, Barbier EB, Silliman BR. 2011. The present and future role of coastal wetland vegetation in protecting shorelines: Answering recent challenges to the paradigm. Climatic Change **106** : 7–29. DOI: 10.1007/s10584-010-0003-7

Gedan KB, Silliman BR, Bertness MD. 2009. Centuries of human-driven change in salt marsh ecosystems. Annual Review of Marine Science **1** : 117–141. DOI: 10.1146/annurev.marine.010908.163930

Grabowski RC. 2014. Measuring the shear strength of cohesive sediment in the field. Geomorphological Techniques **1** : 1–7.

Grabowski RC, Droppo IG, Wharton G. 2011. Erodibility of cohesive sediment: The importance of sediment properties. Earth-Science Reviews **105** : 101–120. DOI: 10.1016/j.earscirev.2011.01.008 [online] Available from: http://dx.doi.org/10.1016/j.earscirev.2011.01.008

Gu J, Luo M, Zhang X, Christakos G, Agusti S, Duarte CM, Wu J. 2018. Losses of salt marsh in China: Trends, threats and management. Estuarine, Coastal and Shelf Science **214** : 98–109. DOI: 10.1016/j.ecss.2018.09.015 [online] Available from: https://doi.org/10.1016/j.ecss.2018.09.015

Gyssels G, Poesen J, Bochet E, Li Y. 2005. Impact of plant roots on the resistance of soils to erosion by water: A review. Progress in Physical Geography **29** : 189–217. DOI: 10.1191/0309133305pp443ra

Helliwell JR, Sturrock CJ, Grayling KM, Tracy SR, Flavel RJ, Young IM, Whalley WR, Mooney SJ. 2013. Applications of X-ray computed tomography for examining biophysical interactions and structural development in soil systems: A review. European Journal of Soil Science **64** : 279–297. DOI: 10.1111/ejss.12028

Hu X, Li XY, Li ZC, Gao Z, Wu X chen, Wang P, Lyu YL, Liu L you. 2020. Linking 3-D soil macropores and root architecture to near saturated hydraulic conductivity of typical meadow soil types in the Qinghai Lake Watershed, northeastern Qinghai–Tibet Plateau. Catena **185** : 104287. DOI: 10.1016/j.catena.2019.104287 [online]

Available from: https://doi.org/10.1016/j.catena.2019.104287

Jarvis N, Larsbo M, Koestel J. 2017. Connectivity and percolation of structural pore networks in a cultivated silt loam soil quantified by X-ray tomography. Geoderma **287** : 71–79. DOI: 10.1016/j.geoderma.2016.06.026 [online] Available from: http://dx.doi.org/10.1016/j.geoderma.2016.06.026

Jolliffe IT. 2002. Principal Component Analysis, Second Edition. Springer Series in Statistics **98** : 487. DOI: 10.1007/b98835 [online] Available from: http://books.google.com/books?id=_olByCrhjwIC%5Cnhttp://www.springerlink.com/index/10.1007/b98835

Katuwal S, Norgaard T, Moldrup P, Lamandé M, Wildenschild D, de Jonge LW. 2015. Linking air and water transport in intact soils to macropore characteristics inferred from X-ray computed tomography. Geoderma **237**–**238** : 9–20. DOI: 10.1016/j.geoderma.2014.08.006 [online] Available from: http://dx.doi.org/10.1016/j.geoderma.2014.08.006

Van de Koppel J, Van der Wal D, Bakker JP, Herman PMJ. 2005. Self-Organization and Vegetation Collapse in Salt Marsh Ecosystems. The American Naturalist **165** : 1–12. DOI: 10.1086/426602

Kristensen E, Kostka JE. 2005. Macrofaunal Burrows and Irrigation in Marine Sediment : Microbiological and Biogeochemical Interactions

Leonardi N, Carnacina I, Donatelli C, Kamal N, James A, Schuerch M, Temmerman S. 2018. Dynamic interactions between coastal storms and salt marshes : A review. Geomorphology **301** : 92–107. DOI: 10.1016/j.geomorph.2017.11.001 [online] Available from: https://doi.org/10.1016/j.geomorph.2017.11.001

Leonardi N, Fagherazzi S. 2015. Local variability in erosional resistance affects large scale morphodynamic response of salt marshes to wind waves and extreme events. Geophysical Research Letters **42** : 5872–5879. DOI: 10.1002/2015GL064730.Received

Li H, Li L, Lockington D. 2005. Aeration for plant root respiration in a tidal marsh. Water Resources Research **41** : 1–11. DOI: 10.1029/2004WR003759

Limaye A. 2012. Drishti: a volume exploration and presentation tool. : 85060X. DOI: 10.1117/12.935640 [online] Available from: http://proceedings.spiedigitallibrary.org/proceeding.aspx?doi=10.1117/12.935640

Lucas M, Schlüter S, Vogel HJ, Vetterlein D. 2019. Roots compact the surrounding soil depending on the structures they encounter. Scientific Reports **9** : 1–13. DOI: 10.1038/s41598-019-52665-w

Lupini A, Araniti F, Mauceri A, Princi M, Di Iorio A, Sorgonà A, Abenavoli MR. 2018. Root morphology. Advances in Plant Ecophysiology Techniques : 15–28. DOI: 10.1007/978-3-319-93233-0_2

Mitsch WJ, Gosselink JG. 1986. Wetlands. : 539.

Möller I et al. 2014. Wave attenuation over coastal salt marshes under storm surge conditions. Nature Geoscience **7** : 727–731. DOI: 10.1038/ngeo2251 [online] Available from: http://www.nature.com/doifinder/10.1038/ngeo2251 (Accessed 30 September 2014)

Müller K, Katuwal S, Young I, McLeod M, Moldrup P, de Jonge LW, Clothier B. 2018. Characterising and linking X-ray CT derived macroporosity parameters to infiltration in soils with contrasting structures. Geoderma **313** : 82–91. DOI:

10.1016/j.geoderma.2017.10.020 [online] Available from: https://doi.org/10.1016/j.geoderma.2017.10.020

Pagenkemper SK, Athmann M, Uteau D, Kautz T, Peth S, Horn R. 2015. The effect of earthworm activity on soil bioporosity - Investigated with X-ray computed tomography and endoscopy. Soil and Tillage Research **146** : 79–88. DOI: 10.1016/j.still.2014.05.007 [online] Available from: http://dx.doi.org/10.1016/j.still.2014.05.007

Pot V, Zhong X, Baveye PC. 2020. Effect of resolution, reconstruction settings, and segmentation methods on the numerical calculation of saturated soil hydraulic conductivity from 3D computed tomography images. Geoderma **362** : 114089. DOI: 10.1016/j.geoderma.2019.114089 [online] Available from: https://doi.org/10.1016/j.geoderma.2019.114089

Priestas AM, Mariotti G, Leonardi N, Fagherazzi S. 2015. Coupled Wave Energy and Erosion Dynamics along a Salt Marsh Boundary, Hog Island Bay, Virginia, USA. Journal of Marine Science and Engineering **3** : 1041–1065. DOI: 10.3390/jmse3031041

Pringle AW. 1995. Erosion of a cyclic saltmarsh In Morecambe Bay, North-West England. Earth Surface Processes and Landforms **20** : 387–405.

Pulido-Moncada M, Katuwal S, Ren L, Cornelis W, Munkholm L. 2020. Impact of potential bio-subsoilers on pore network of a severely compacted subsoil. Geoderma **363** : 114154. DOI: 10.1016/j.geoderma.2019.114154 [online] Available from: https://doi.org/10.1016/j.geoderma.2019.114154

Van Putte N, Temmerman S, Verreydt G, Seuntjens P, Maris T, Heyndrickx M, Boone M, Joris I, Meire P. 2019. Groundwater dynamics in a restored tidal marsh are

limited by historical soil compaction. Estuarine, Coastal and Shelf Science : 106101. DOI: 10.1016/j.ecss.2019.02.006 [online] Available from: https://doi.org/10.1016/j.ecss.2019.02.006

Rabot E, Wiesmeier M, Schlüter S, Vogel HJ. 2018. Soil structure as an indicator of soil functions: A review. Geoderma **314** : 122–137. DOI: 10.1016/j.geoderma.2017.11.009 [online] Available from: https://doi.org/10.1016/j.geoderma.2017.11.009

Redelstein R, Dinter T, Hertel D, Leuschner C. 2018. Effects of inundation, nutrient availability and plant species diversity on fine root mass and morphology across a saltmarsh flooding gradient. Frontiers in Plant Science **9** : 1–15. DOI: 10.3389/fpls.2018.00098

Reid MK, Spencer KL. 2009. Use of principal components analysis (PCA) on estuarine sediment datasets: The effect of data pre-treatment. Environmental Pollution **157** : 2275–2281. DOI: 10.1016/j.envpol.2009.03.033 [online] Available from: http://dx.doi.org/10.1016/j.envpol.2009.03.033

Rowell DL. 1994. Soil science: methods and applications. . Longman Group Limited, Longman Scientific & Technical

Schindelin J et al. 2012. Fiji: An open-source platform for biological-image analysis. Nature Methods **9** : 676–682. DOI: 10.1038/nmeth.2019

Schwimmer RA. 2001. Rates and processes of marsh shoreline erosion in Rehoboth Bay, Delaware, U.S.A. Journal of Coastal Research **17** : 672–683.

Spencer KL, Carr SJ, Diggens LM, Tempest JA, Morris MA, Harvey GL. 2017. The impact of pre-restoration land-use and disturbance on sediment structure, hydrology

and the sediment geochemical environment in restored saltmarshes. Science of the Total Environment **587**–**588** : 47–58. DOI: 10.1016/j.scitotenv.2016.11.032

Steel TJ. 1996. The morphology and development of representative British saltmarsh creek networks

Tempest J a., Harvey GL, Spencer KL. 2015. Modified sediments and subsurface hydrology in natural and recreated salt marshes and implications for delivery of ecosystem services. Hydrological Processes **29** : 2346–2357. DOI: 10.1002/hyp.10368 [online] Available from: http://doi.wiley.com/10.1002/hyp.10368

Tracy SR, Daly KR, Sturrock CJ, Crout NMJ, Mooney SJ, Roose T. 2015. Three-dimensional quantification of soil hydraulic properties using X-ray Computed Tomography and image-based modeling. Water Resources Research **51** : 1006–1022. DOI: 10.1002/2014WR016259

Vannoppen W, Vanmaercke M, De Baets S, Poesen J. 2015. A review of the mechanical effects of plant roots on concentrated flow erosion rates. Earth-Science Reviews **150** : 666–678. DOI: 10.1016/j.earscirev.2015.08.011

Vogel H-J. 1997. Digital unbiased estimation of the Euler-Poincaré characteristic in different dimensions. Acta stereologica **16** : 97–104.

Vu HD, Wieski K, Pennings SC. 2017. Ecosystem engineers drive creek formation in salt marshes. Ecology **98** : 162–174. DOI: 10.1002/ecy.1628

Van der Wal D, Wielemaker-Van den Dool A, Herman PMJ. 2008. Spatial patterns, rates and mechanisms of saltmarsh cycles (Westerschelde, The Netherlands). Estuarine, Coastal and Shelf Science **76** : 357–368. DOI: 10.1016/j.ecss.2007.07.017

Wang H, van der Wal D, Li X, van Belzen J, Herman PMJ, Hu Z, Ge Z, Zhang L, Bouma TJ. 2017. Zooming in and out: Scale dependence of extrinsic and intrinsic factors affecting salt marsh erosion. Journal of Geophysical Research: Earth Surface **122** : 1455–1470. DOI: 10.1002/2016JF004193

Wiberg PL, Law BA, Wheatcroft RA, Milligan TG, Hill PS. 2012. Seasonal variations in erodibility and sediment transport potential in a mesotidal channel-flat complex, Willapa Bay, WA. Continental Shelf Research **60** : 185–197. DOI: 10.1016/j.csr.2012.07.021

Williams B, Onsman A, Brown T. 2010. Exploratory factor analysis: A five-step guide for novices. Journal of Emergency Primary Health Care **8** : 1–13. DOI: 10.33151/ajp.8.3.93

Xin P, Jin G, Li L, Barry DA. 2009. Effects of crab burrows on pore water flows in salt marshes. Advances in Water Resources **32** : 439–449. DOI: 10.1016/j.advwatres.2008.12.008 [online] Available from: http://linkinghub.elsevier.com/retrieve/pii/S0309170808002303

Table 1: List of variables considered when interpreting the µCT data, with their definition and corresponding structural parameters when applied to pores and organic matter elements

Variable	Definition	Pore parameter	Organic matter parameter
Total phase fraction (%)	Fraction of the number of voxels belonging to a phase by the total number of voxels in the volume	Pore fraction (porosity as a percentage of the total sample volume)	Organic fraction
Number of objects / particles	Number of individual connected clusters of voxels (= objects or particles) in a phase, detected using a 26-voxel connectivity using the Particle Analysis plugin in ImageJ	Number of connected pore systems	Number of connected organic matter elements
Connectivity (%)	Volume of the largest connected particle divided by the total volume of the studied phase (how much of the total phase belongs to a single connected system)	Connectivity of the pore system	Connectivity of the root system
Emptiness (mm)	Mean distance between voxels of the same phase	Mean distance between pores	Mean distance between organic matter elements
Euler Poincaré characteristic	Topological invariant that describes the shape or structure of a topological space (Vogel, 1997), calculated using the Particle Analysis plugin in ImageJ. A value of 0 means a perfectly simple (i.e. one single pore/root), and the further the value deviates from 0, the greater the topological complexity of the phase.	Complexity of the pore system	Complexity of the root system
Mean Thickness (µm)	Mean value of the local thickness (Particle Analysis plugin in ImageJ), measured at each point in a particle as the diameter of the greatest sphere that fits within the particle and which contains the point	Pore mean thickness	Mean thickness of organic matter elements

Table 2: Summary table for all datasets

Variable	CT morphological parameters	Organic Matter (%)	% clay material	Sodium Adsorption Ratio	Shear Strength (kPa)
Sample type	Undisturbed sediment core	Disturbed sediment core			Distributed survey across a large area of the marsh
Date collected	Jan 2019	Jan 2019			Aug-Sept 2019
Method	Computed Tomography	Loss on Ignition	Particle Size Analysis	Exchanged cation analysis	Shear vane
Sampling frequency and depth per station	3-4 replicates cores (15cm)	1 core, 15 measurements (every 1cm)	1 core, 7-8 measurements (every 2cm)	2 measurements (at 0.5 and 7.5cm) for each 3 replicates	150 measurements (at 7.5cm)

Table 3: Description of pores and organic matter elements appearance at each station (TF = Tillingham Farm; WS = Warton Sands; BG = Bare Ground; PUC = *Puccinellia spp*; SAL = *Salicornia spp*; SPA = *Spartina spp*; PORES = pores; ORGS = organic matter elements)

	PORES appearance	ORGS appearance
TF BG	Large and complex pore system through the whole core, dominantly vertical, highly connected. The diameter of the pores matches that of *Spartina spp* roots in other samples	Small number of scattered, small and roundish organic particles. No live root system.
WS BG	Regularly spaced small vertical tubular pores at the bottom of the sample, characteristic of a buried bioturbation horizon	Few scattered tubular organic particles. No live root system.
TF PUC	Internal cracks with a preferential horizontal orientation	Dense mat of thin roots with a preferential horizontal orientation. Live root system highly fibrous.
WS PUC	Internal cracks with no preferential orientation; thin tubular voids	Dense mat of thin roots with no preferential orientation. Live root system highly fibrous
TF SAL	Thick, tubular, interconnected and complex pore network with a preferential vertical orientation. The diameter of the pores matches that of *Spartina spp* roots in other samples.	Combination of thicker roots with a preferential horizontal orientation, and of a loose mesh of thinner roots with no preferential orientation. Live root system appears fibrous. Several species are likely to coexist (most *Salicornia*-dominated spots at Tillingham also contained some *Puccinellia spp*)
WS SAL	Buried horizons of extremely regular vertical or looping burrows, horizontal cracks in the sediment	Thin roots or buried stems joining at depth into one tap root with a vertical orientation, surrounded by a very loose mesh of thinner roots. Root system type: tap root.
TF SPA	Thick, tubular, interconnected and complex pore network with a preferential vertical orientation; round holes caused by hollow shells	Thick curved roots, with a preferential vertical orientation, abundant at the surface but growing sparser with depth, surrounded by a loose mesh of thinner roots with a preferential vertical orientation. Root system type: tap root.
WS SPA	Straight tubular pores with a strong preferential vertical orientation through the whole core; small elongated vertical pores in the lower half	Thick straight roots piercing vertically through the whole core, surrounded by small elongated vertical organic matter elements in the lower half. Root system type: tap root.

Table 4: Topology of the macropores at all stations. Mean values of all core replicates (standard deviation in brackets). Spider plot values have been normalised to the interval 0-1.

PORES	Total phase fraction (%)	Number of particles	Connectivity (%)	Emptiness (mm)	Euler Poincaré characteristic (absolute value)	Mean Thickness (µm)
TF BG	8.06 *(0.79)*	1140 *(228)*	46.4 *(18.6)*	1.07 *(0.05)*	2298 *(2094)*	1108 *(59)*
TF PUC	3.94 *(1.55)*	614 *(96)*	52.0*(30.0)*	2.50 *(0.43)*	8967 *(5689)*	643 *(14)*
TF SAL	5.73 *(0.67)*	1330 *(267)*	63.1 *(9.0)*	1.51 *(0.37)*	3744 *(261)*	729 *(55)*
TF SPA	7.09 *(0.94)*	817 *(34)*	73.2 *(4.3)*	1.33 *(0.15)*	17136 *(4034)*	876 *(111)*
WS BG	0.60 *(0.28)*	401 *(97)*	3.9 *(0.6)*	14.95 *(6.45)*	66 *(34)*	852 *(74)*
WS PUC	1.12 *(0.80)*	959 *(285)*	51.1 *(24.4)*	3.18 *(1.40)*	4637 *(3241)*	410 *(81)*
WS SAL	3.14 *(1.13)*	703 *(112)*	36.9 *(13.3)*	3.32 *(0.62)*	5288 *(2438)*	698 *(50)*
WS SPA	2.64 *(0.70)*	725 *(244)*	38.5 *(15.7)*	3.01 *(0.54)*	14967 *(4884)*	705 *(43)*

Table 5: Topology of the organic matter elements at all stations. Mean values of all core replicates (standard deviation in brackets). Spider plot values have been normalised to the interval 0-1.

ORGS	Total phase fraction (%)	Number of particles	Connectivity (%)	Emptiness (mm)	Euler Poincaré characteristic (absolute value)	Mean Thickness (µm)
TF BG	0.18 *(0.05)*	701 *(163)*	27.83 *(15.00)*	3.48 *(0.80)*	300 *(161)*	509 *(20)*
TF PUC	2.72 *(0.55)*	3617 *(537)*	31.71 *(16.99)*	0.80 *(0.16)*	9942 *(9167)*	534 *(17)*
TF SAL	1.06 *(0.48)*	2501 *(763)*	20.48 *(9.48)*	1.26 *(0.25)*	3271 *(3924)*	514 *(18)*
TF SPA	2.92 *(1.20)*	1853 *(664)*	73.47 *(5.95)*	1.31 *(0.47)*	26360 *(3632)*	502 *(15)*
WS BG	0.05 *(0.03)*	221 *(132)*	5.31 *(3.48)*	17.30 *(5.24)*	191 *(208)*	441 *(43)*
WS PUC	2.32 *(1.33)*	3465 *(278)*	24.44 *(32.37)*	0.96 *(0.26)*	24396 *(33884)*	523 *(38)*
WS SAL	0.44 *(0.27)*	781 *(410)*	20.89 *(14.37)*	4.79 *(2.91)*	4540 *(4115)*	467 *(16)*
WS SPA	2.30 *(0.49)*	1559 *(280)*	64.54 *(6.04)*	1.75 *(0.19)*	34258 *(6403)*	558 *(51)*

Table 6: Mean results per ground cover and sediment type for % of clay material, % of organic matter, Sodium Adsorption Ratio and Shear Strength (standard deviation in brackets).

	% < 63 µm	Organic Matter	SAR	Shear Strength
TF BG	96.5 *(2.9)*	6.7 *(1.0)*	55.8 *(8.3)*	20.6 *(4.9)*
TF PUC	88.1 *(7.9)*	15.0 *(1.9)*	49.5 *(1.7)*	27.3 *(6.0)*
TF SAL	86.0 *(6.1)*	9.3 *(1.5)*	45.7 *(1.7)*	22.5 *(7.0)*
TF SPA	89.8 *(2.4)*	7.7 *(1.2)*	58.7 *(13.7)*	22.4 *(6.7)*
WS BG	46.8 *(9.5)*	2.3 *(0.3)*	29.5 *(3.7)*	31.1 *(17.4)*
WS PUC	57.1 *(7.5)*	2.5 *(0.8)*	21.5 *(1.5)*	68.2 *(16.8)*
WS SAL	65.3 *(10.0)*	2.9 *(0.6)*	24.6 *(1.5)*	47.4 *(17.6)*
WS SPA	51.7 *(6.9)*	3.1 *(0.5)*	37.1 *(7.8)*	42.3 *(18.4)*

Table 7: Comparison of p-values for Kruskal-Wallis tests for the organic matter content, percentage of particles below 63 microns, sodium adsorption ratio and shear strength for each ground cover and sediment type (p<0.05 means two groups are significantly different, with blue and yellow highlights denoting significant or non-significant differences).

Organic Matter	TFPUC	TFSAL	TFSPA	WSBG	WSPUC	WSSAL	WSSPA
TFBG	0.041949	0.856539	0.963948	0.00433	0.007617	0.248141	0.135231
TFPUC		0.695476	0.464693	6.01E-08	6.04E-08	1.26E-06	3.05E-07
TFSAL			0.999976	7.02E-06	1.55E-05	0.003787	0.001262
TFSPA				3.96E-05	8.31E-05	0.013041	0.004837
WSBG					1	0.872087	0.958265
WSPUC						0.927422	0.981847
WSSAL							0.999994
%<63µm	TFPUC	TFSAL	TFSPA	WSBG	WSPUC	WSSAL	WSSPA
TFBG	0.790961	0.767856	0.775679	4.57E-06	0.000119	0.003262	0.000222
TFPUC		1	1	0.005185	0.045695	0.295596	0.067284
TFSAL			1	0.006029	0.051449	0.318447	0.07521
TFSPA				0.005734	0.049466	0.310726	0.072487
WSBG					0.998237	0.853102	0.994203
WSPUC						0.994793	1
WSSAL							0.99846
SAR	TFPUC	TFSAL	TFSPA	WSBG	WSPUC	WSSAL	WSSPA
TFBG	0.99995	0.805	1	0.03229	0.000362	0.01245	0.5243
TFPUC		0.9494	0.99969	0.09384	0.001772	0.04158	0.77013
TFSAL			0.73279	0.70671	0.084119	0.51004	0.99987
TFSPA				0.02174	0.000206	0.00802	0.4399
WSBG					0.939059	0.99999	0.92092
WSPUC						0.98732	0.23505
WSSAL							0.79366
Shear Strength	TFPUC	TFSAL	TFSPA	WSBG	WSPUC	WSSAL	WSSPA
TFBG	1.71E-06	0.983641	0.838997	2.70E-07	5.99E-08	5.99E-08	5.99E-08
TFPUC		0.00016	0.001428	0.999951	5.99E-08	5.99E-08	7.73E-07
TFSAL			0.999598	2.78E-05	5.99E-08	5.99E-08	5.99E-08
TFSPA				0.000295	5.99E-08	5.99E-08	5.99E-08
WSBG					5.99E-08	5.99E-08	5.81E-06
WSPUC						2.74E-07	5.99E-08
WSSAL							0.394279

Table 8: Principal Components loadings (variables whose loadings exceed ±0.40 are considered important determinants of the variability in the dataset and shaded in red)

	PC1	PC2	PC3
'PORE Fraction (%)'	-0.38	0.42	-0.01
'ORGS Fraction (%)'	-0.05	-0.18	0.42
PORE nb particles	-0.43	-0.03	-0.20
ORGS nb particles	-0.28	-0.41	0.00
'PORE Emptiness'	0.46	-0.03	-0.02
'ORGS Emptiness'	0.42	0.14	-0.07
PORE % Connectivity	-0.39	0.10	0.06
ORGS % Connectivity	0.01	0.19	0.55
PORE Euler	-0.06	0.08	0.45
ORGS Euler	0.09	-0.10	0.49
‘PORE thickness’	0.02	0.57	-0.04
‘ORGS thickness’	-0.18	-0.11	0.14
'Shear Strength'	0.01	-0.45	-0.04

Appendix Table 1: p-values for Kolmogorov-Smirnov test for normality, Bartlett and Levene for homoscedasticity for the clay fraction, organic matter content, sodium adsorption ratio and shear strength (p<0.05 means two groups are significantly different, with blue and yellow highlights denoting significant or non-significant differences).

	Kolmogorov-Smirnov test p-value			
	% < 63 µm	OM	SAR	Shear Strength
TFBG	0.657	0.454	0.764	0.245
TFPUC	0.644	0.515	0.980	0.093
TFSAL	0.690	0.708	0.954	0.172
TFSPA	0.456	0.689	0.276	0.188
WSBG	0.472	0.898	0.197	0.004
WSPUC	0.932	0.582	0.985	0.041
WSSAL	0.808	0.655	0.560	0.317
WSSPA	0.943	0.042	0.509	0.143
Bartlett test p-value	0.006	1.68E-09	1.10E-06	6.84E-88

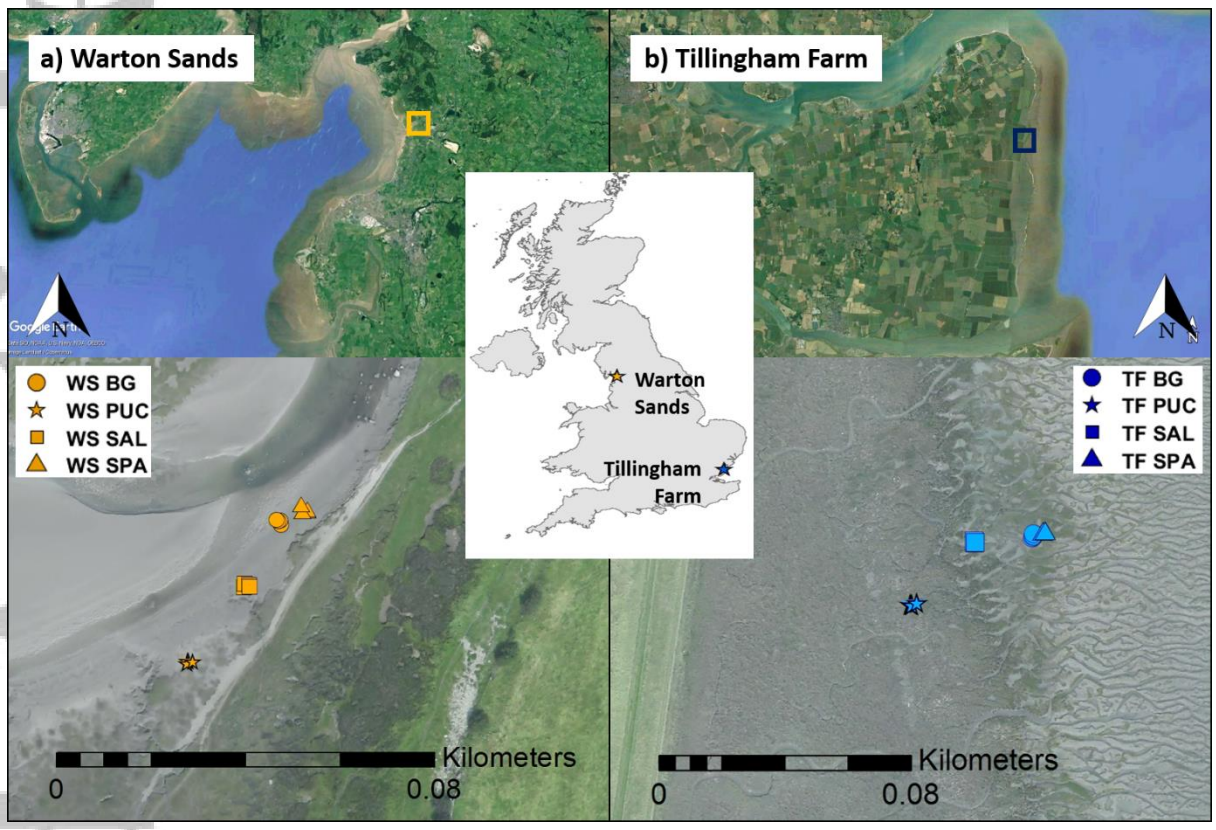

Figure 1: ArcGIS map of the sediment core sample stations. Left = Warton Sands (WS, 2° 47' 27.17" W 54° 7' 43.003" N). Right = Tillingham Farm (TF, 0° 56' 31.148" E 51° 41' 50.697" N). BG = Bare Ground. PUC = Puccinellia. SAL = Salicornia. SPA = Spartina.

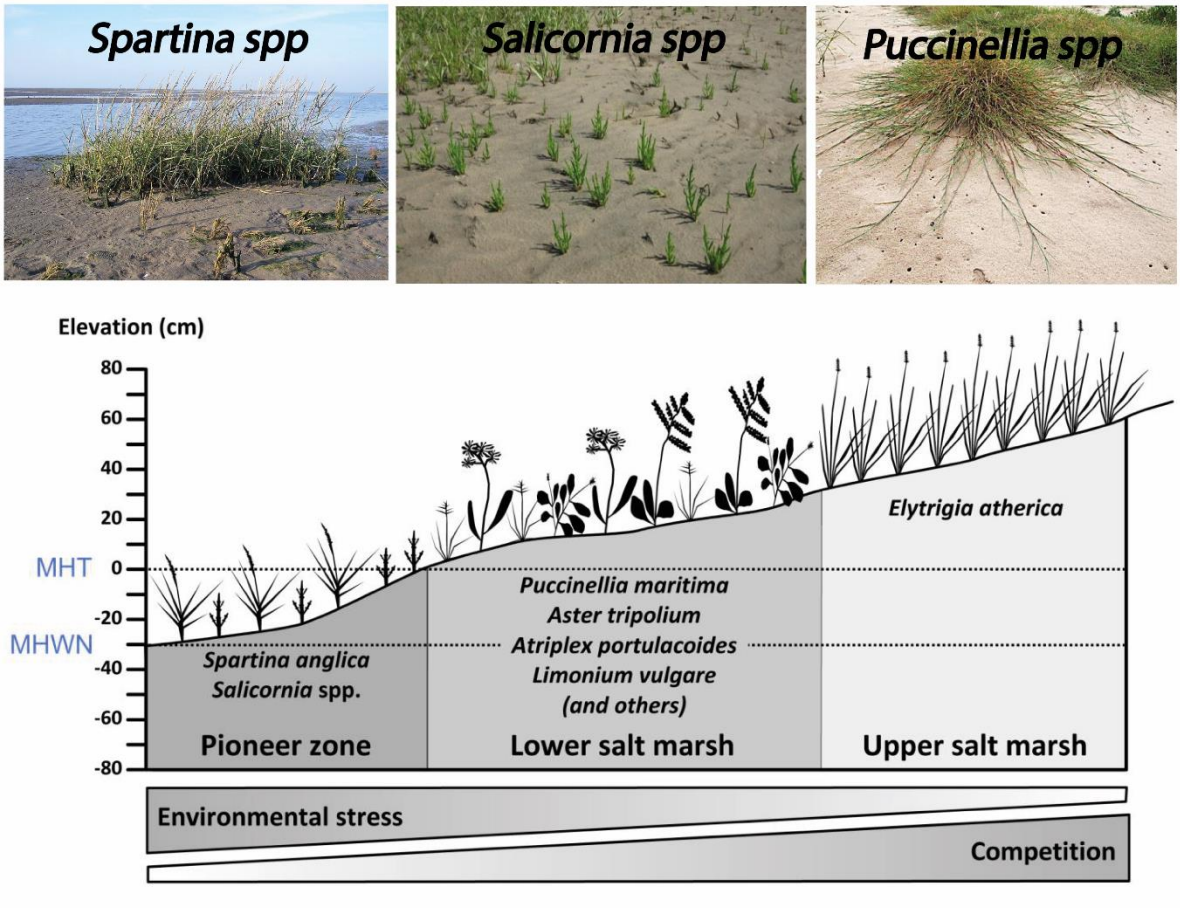

Figure 2: Plant zonation in N-W Europe saltmarshes (Redelstein et al., 2018)

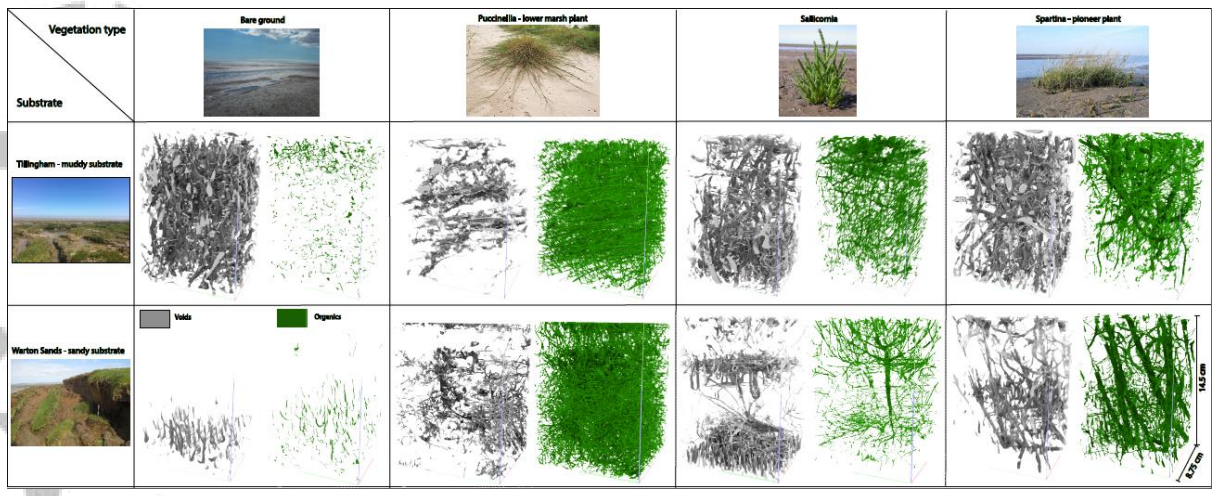

Figure 3: 3D visualisation of pores and organic matter elements for all stations.

Sample size = 8.75*8.75 *14.5 cm. (See Appendix 1 for a visualisation of replicates)

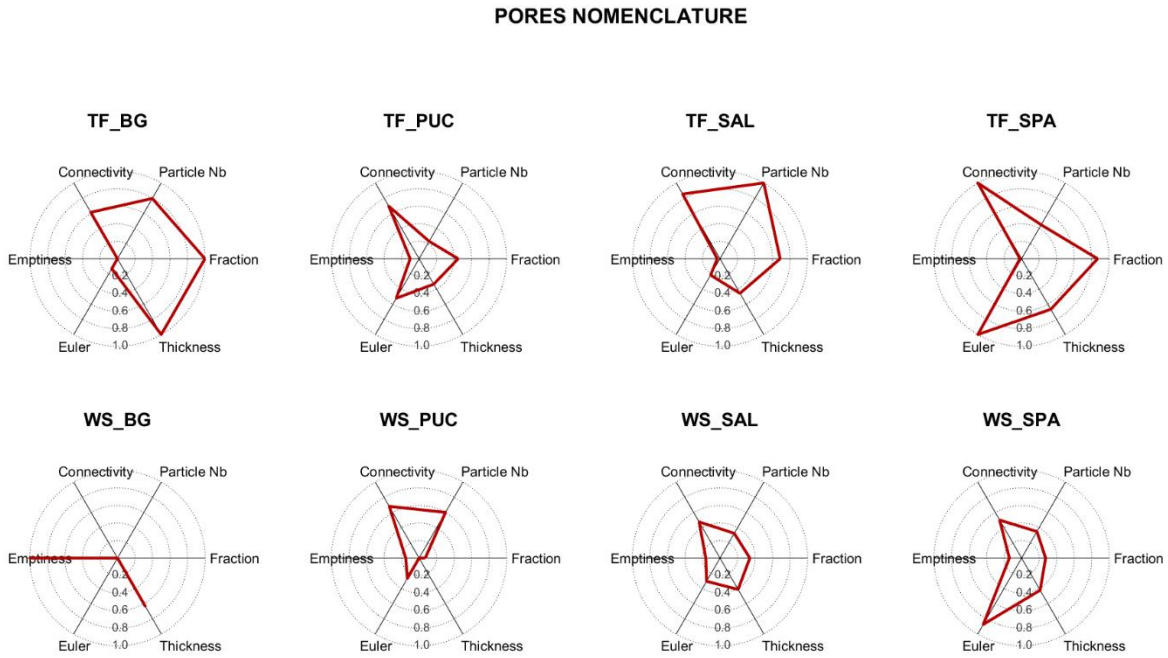

Figure 4: Spider plot representation of the topology of the macropores at all stations. Spider plot values have been normalised to the interval 0-1.

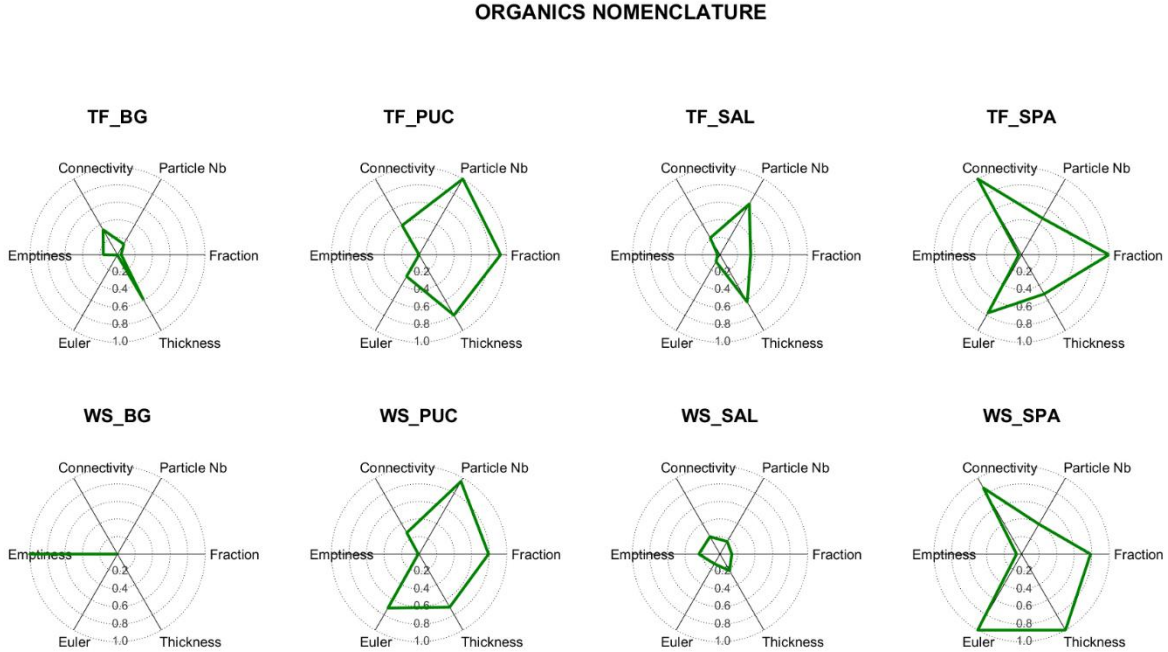

Figure 5: Spider plot representation of the topology of the organic matter elements at all stations. Spider plot values have been normalised to the interval 0-1.

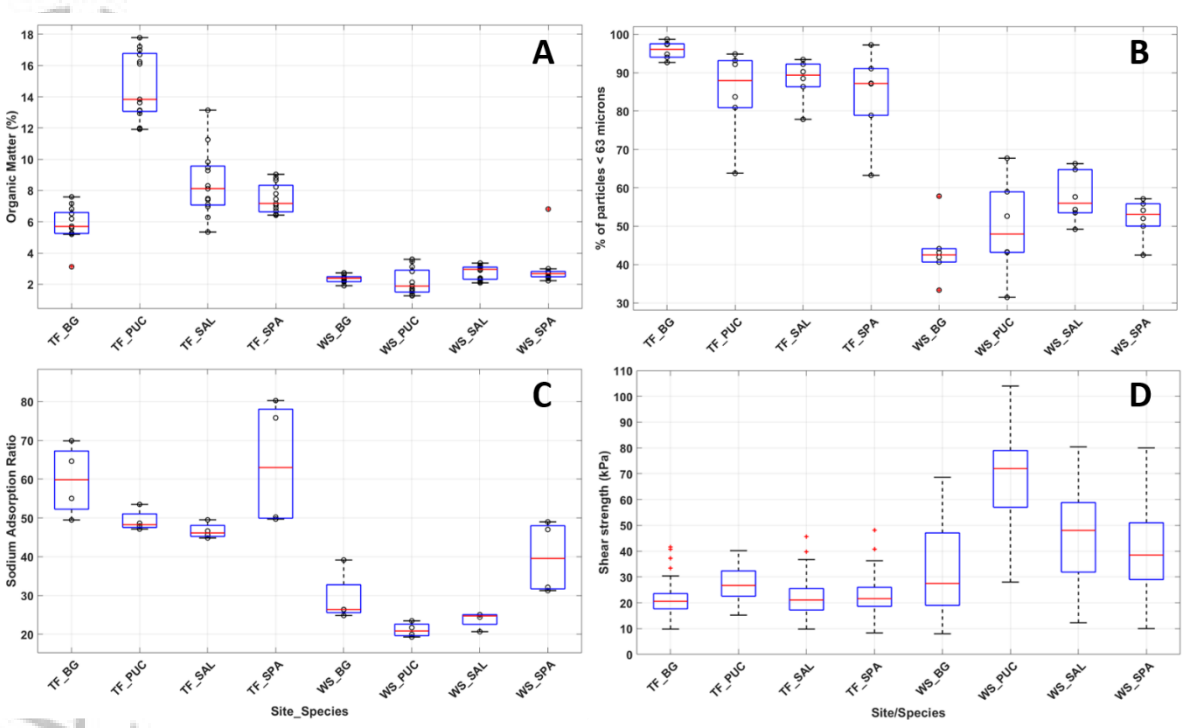

Figure 6: Box plots showing the distribution of A: organic matter content (%); B: percentage of particles below 63 microns (%); C: sodium adsorption ratio (no unit) and D: shear strength (kPa) for each ground cover and sediment type. Black circles represent the individual measurements for each box plot (see Table 2 for the sampling strategy and number of data points for each data type).

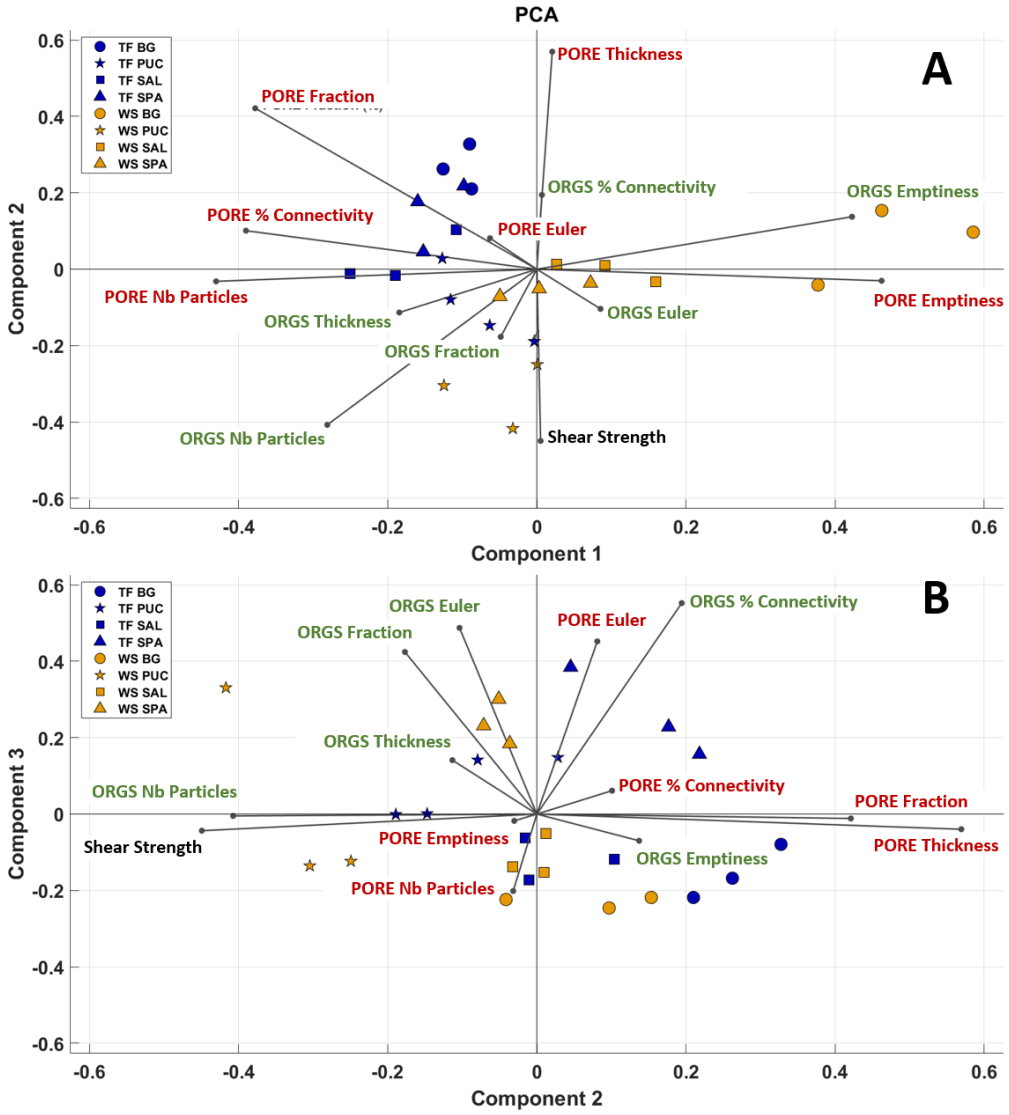

Figure 7: Biplot of the PCA. A: PC 1 and 2; B: PC 2 and 3. Pore parameters are represented in red, organic parameters in green, and the shear strength in black.

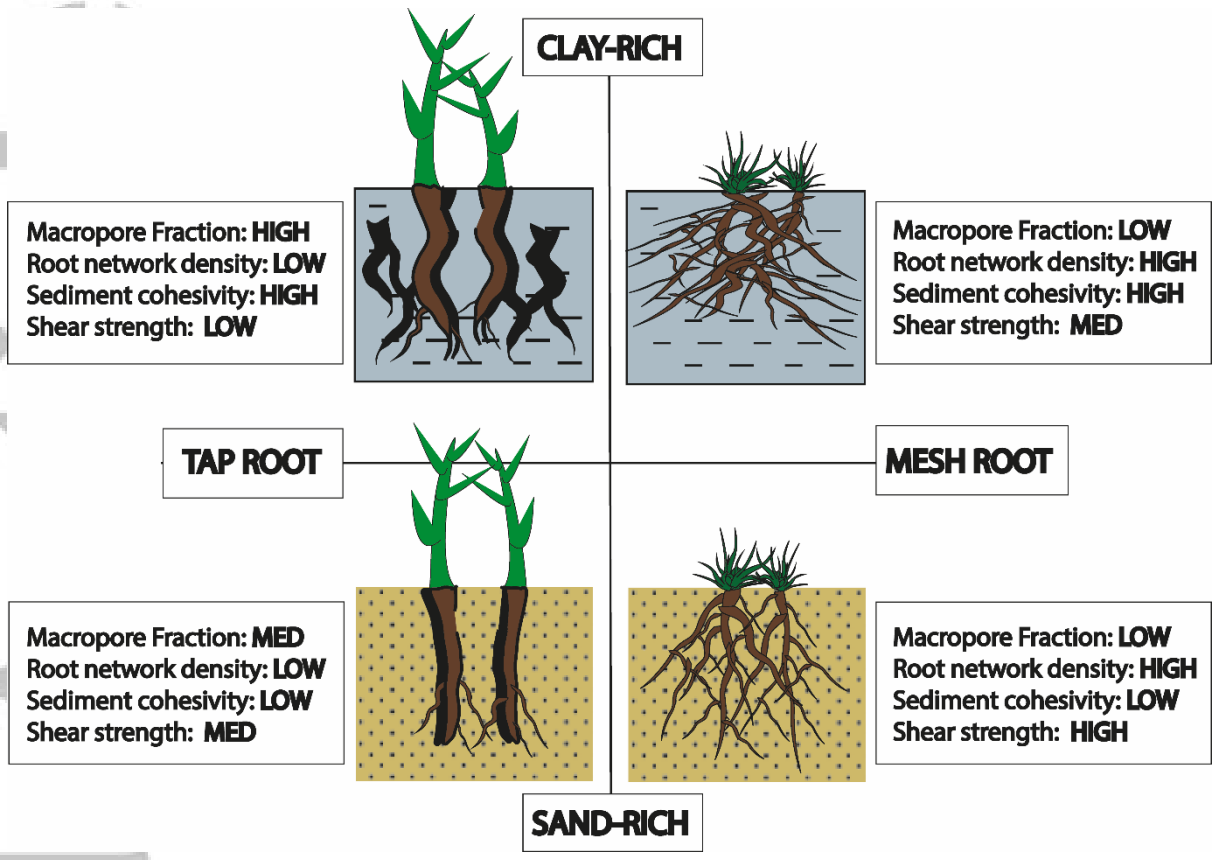

Figure 8: Schematic representation of root and macropore characteristics in different substrates and associated shear strength

Appendix 1a: Tillingham Farm, bare ground (top to bottom: TF BG1, TF BG2, TF BG3)

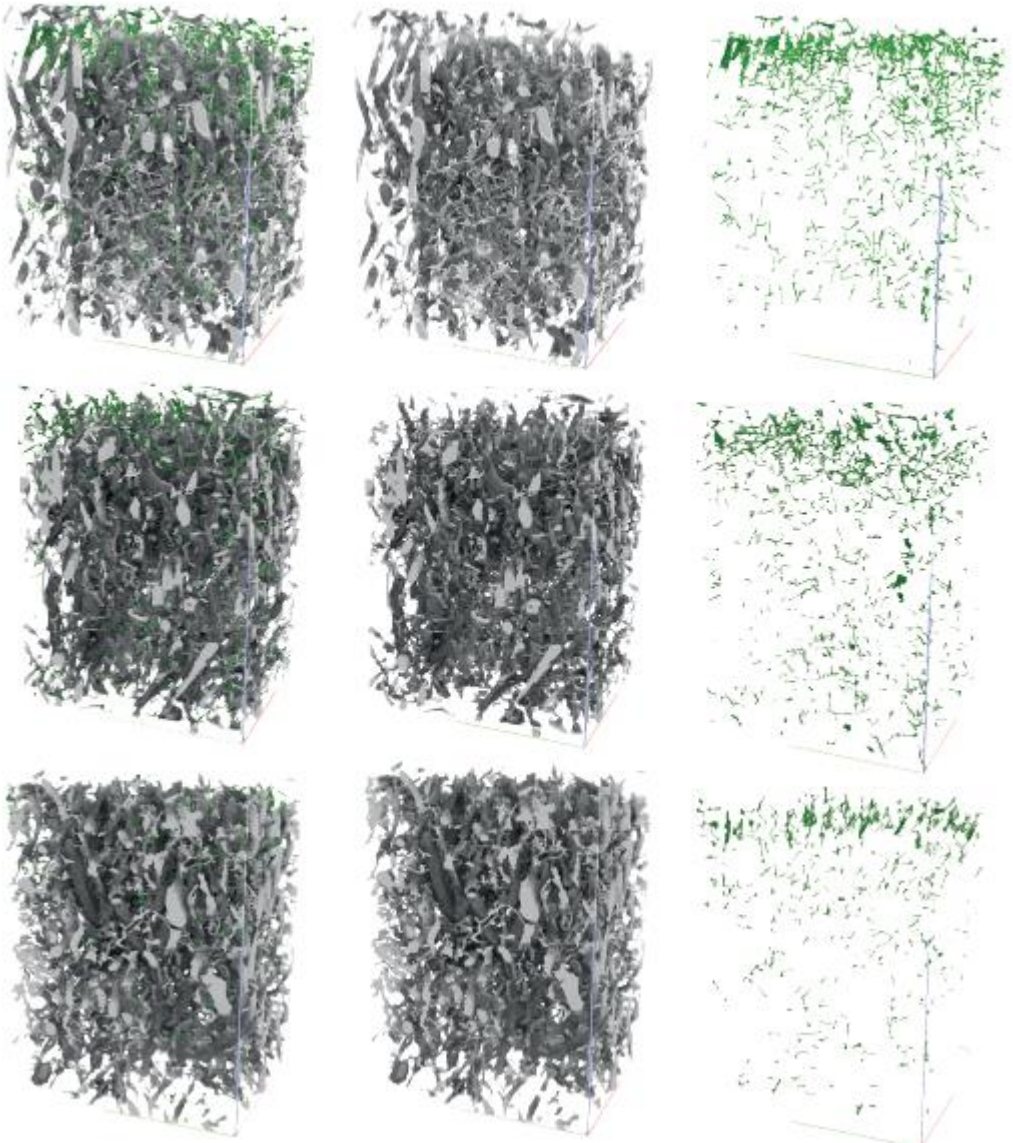

Appendix 1b: Warton Sands, bare ground (top to bottom: WS BG1, WS BG2, WS BG3)

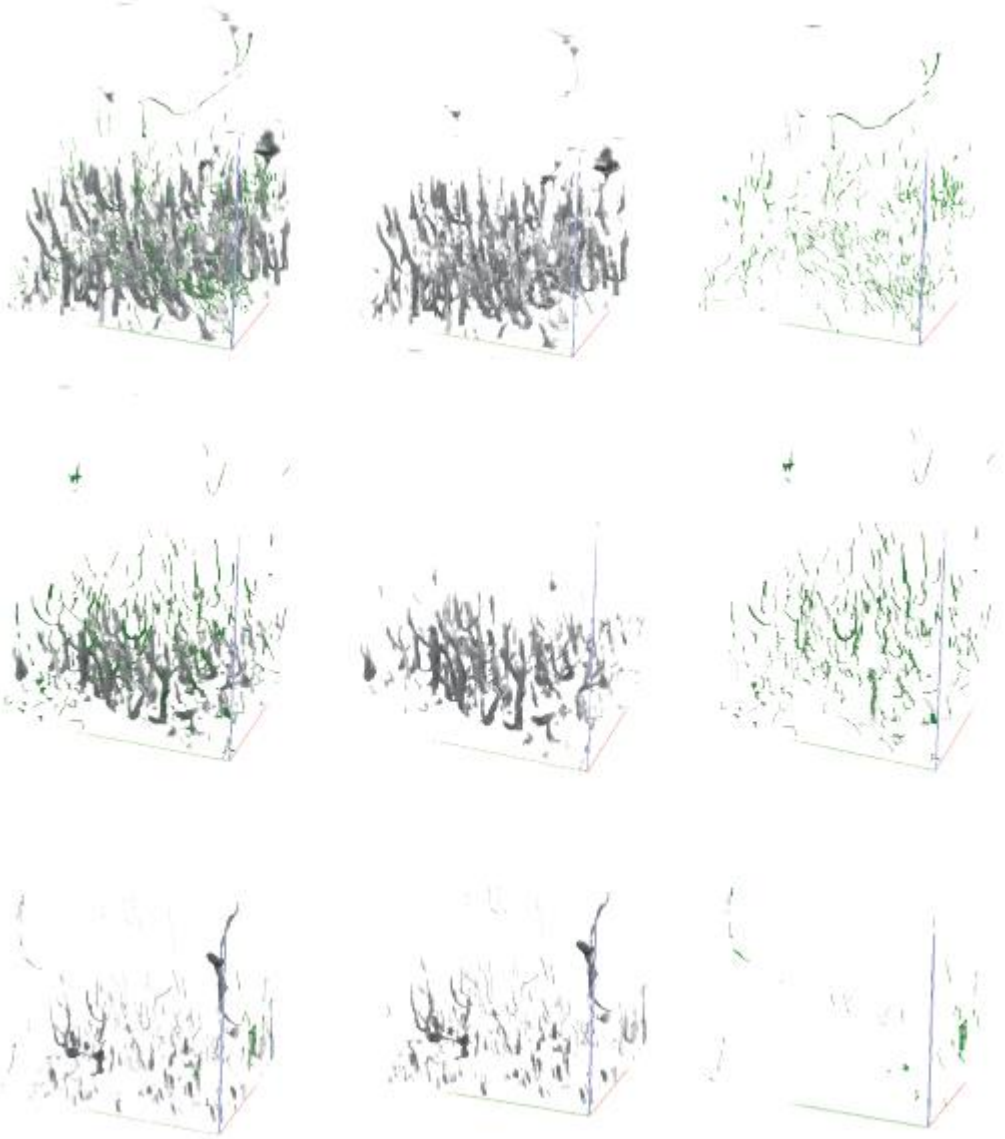

Appendix 1c: Tillingham Farm, *Puccinellia spp* (top to bottom: TF PUC1, TF PUC2, TF PUC3)

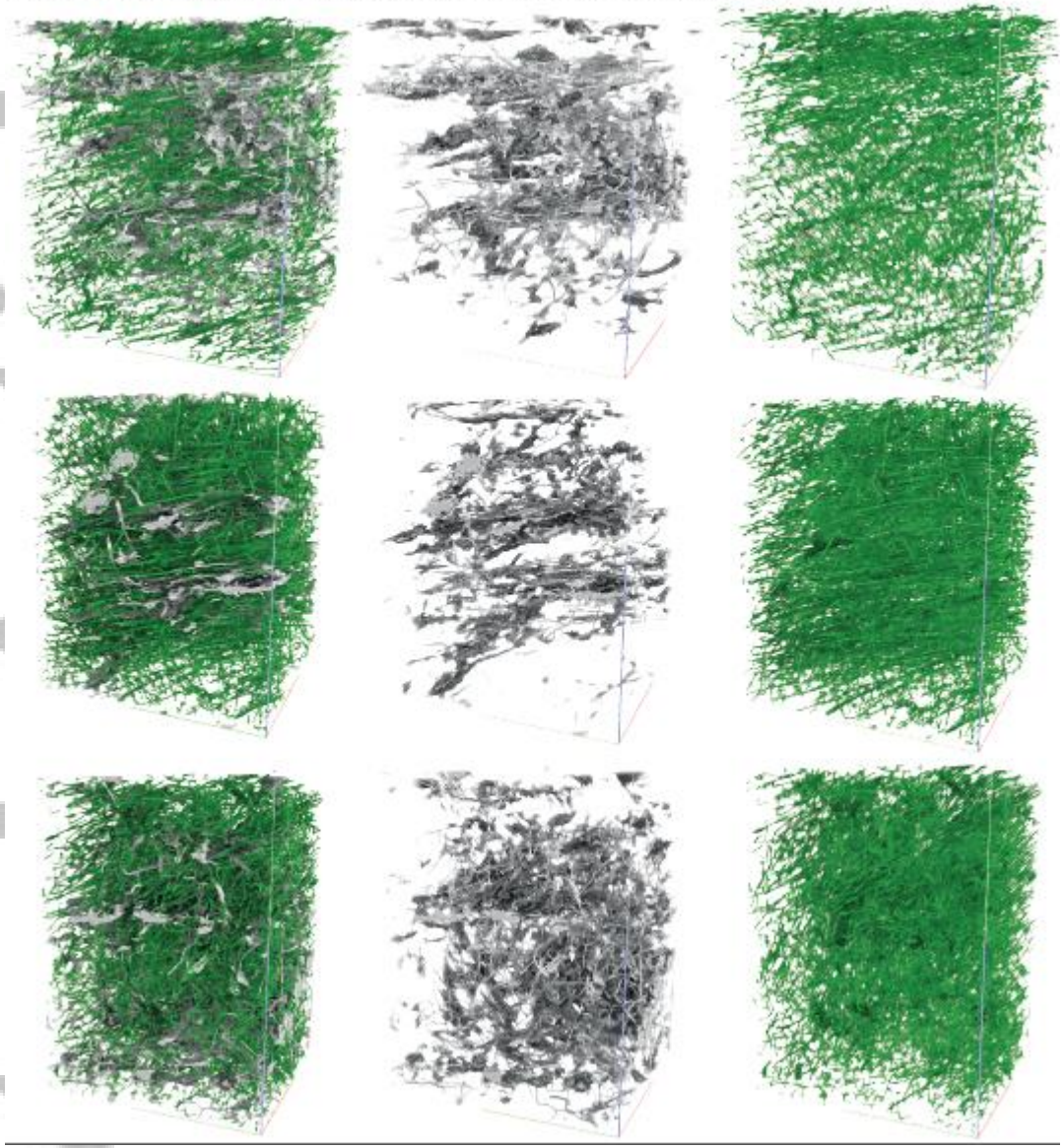

Appendix 1d: Warton Sands, *Puccinellia spp* (top to bottom: WS PUC1, WS PUC2, WS PUC3)

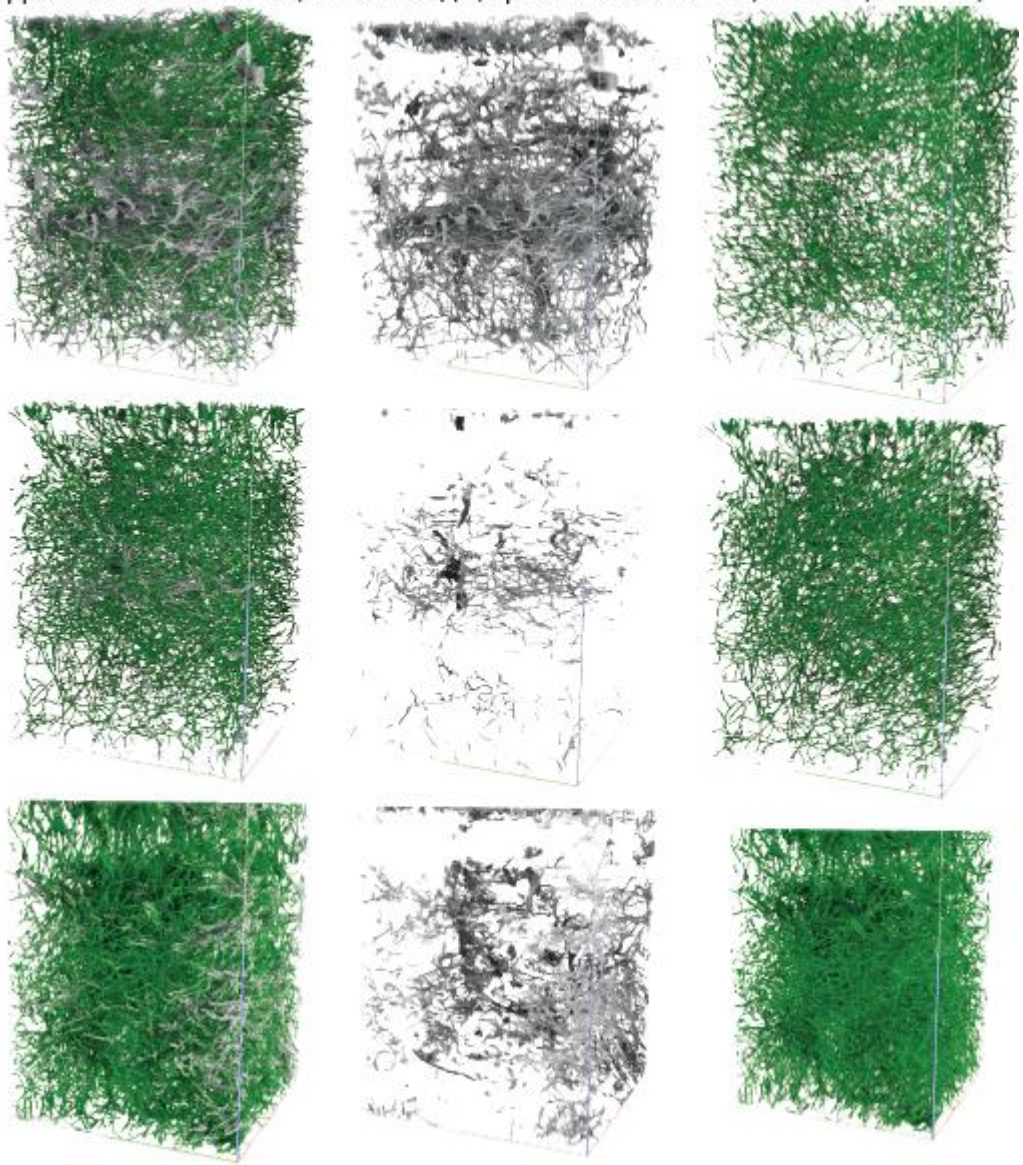

Appendix 1e: Tillingham Farm, *Salicornia spp* (top to bottom: TF SAL1, TF SAL2, TF SAL3)

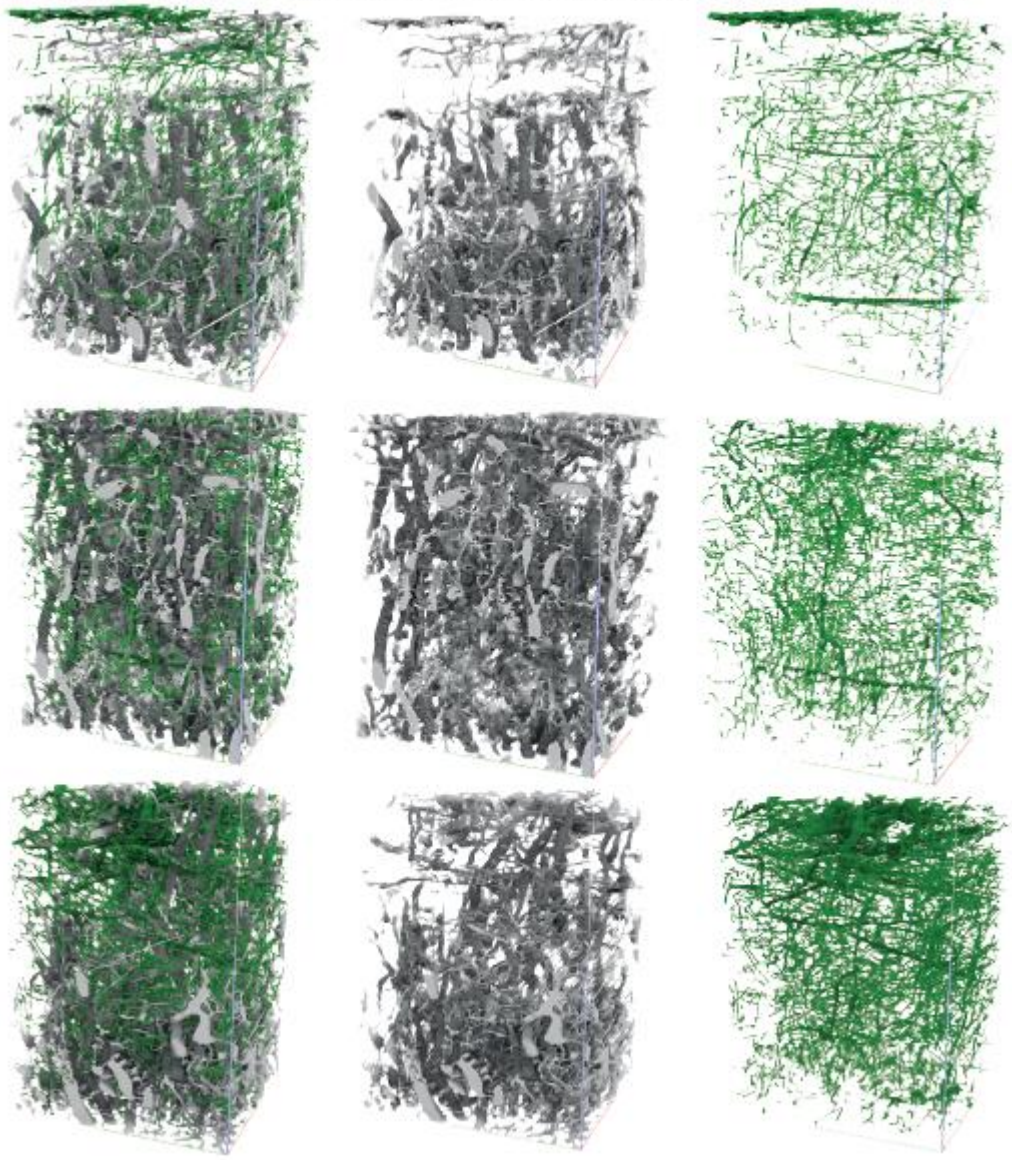

Appendix 1f: Warton Sands, *Salicornia spp* (top to bottom: WS SAL1, WS SAL2, WS SAL3)

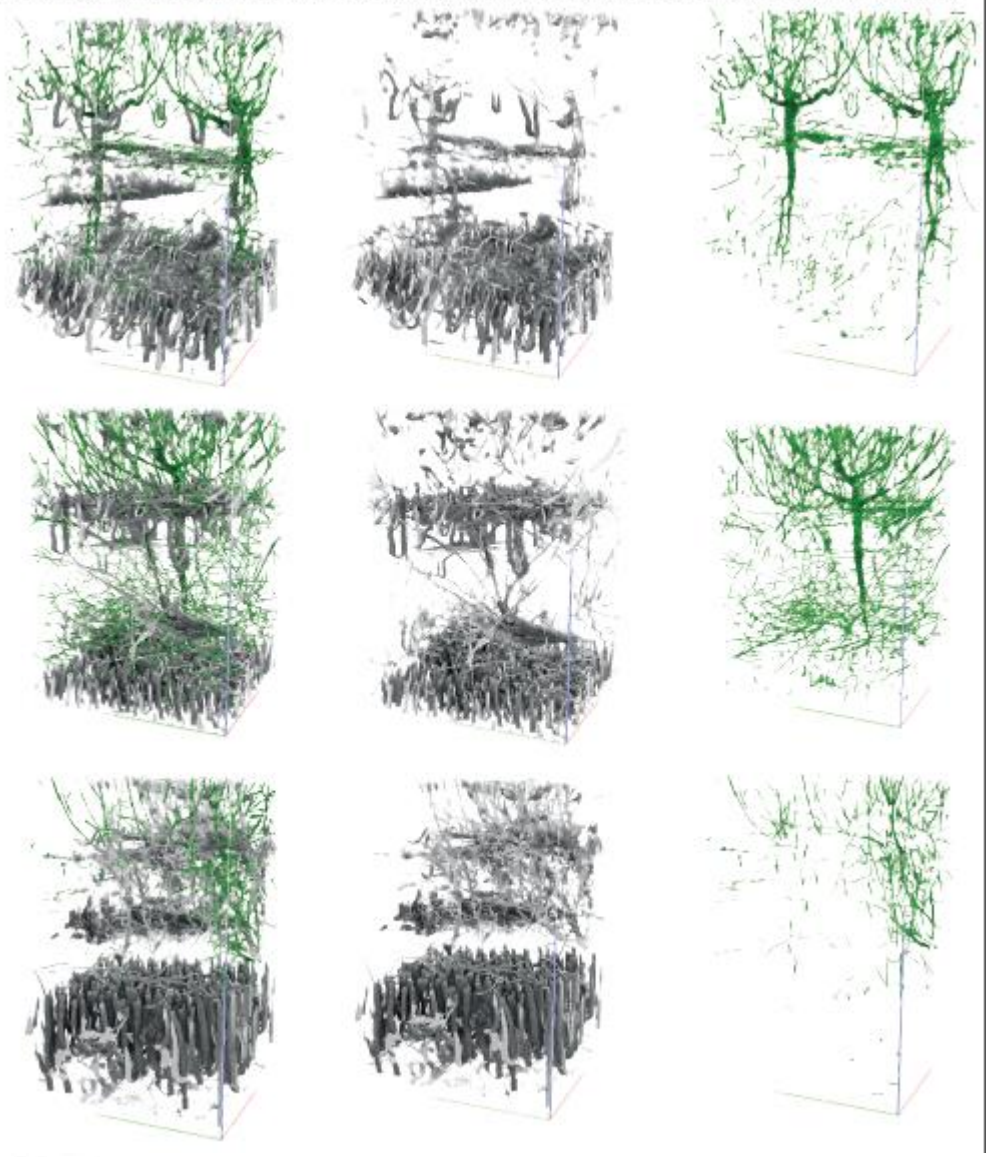

Appendix 1g: Tillingham Farm, *Spartina spp* (top to bottom: TF SPA1, TF SPA2, TF SPA3)

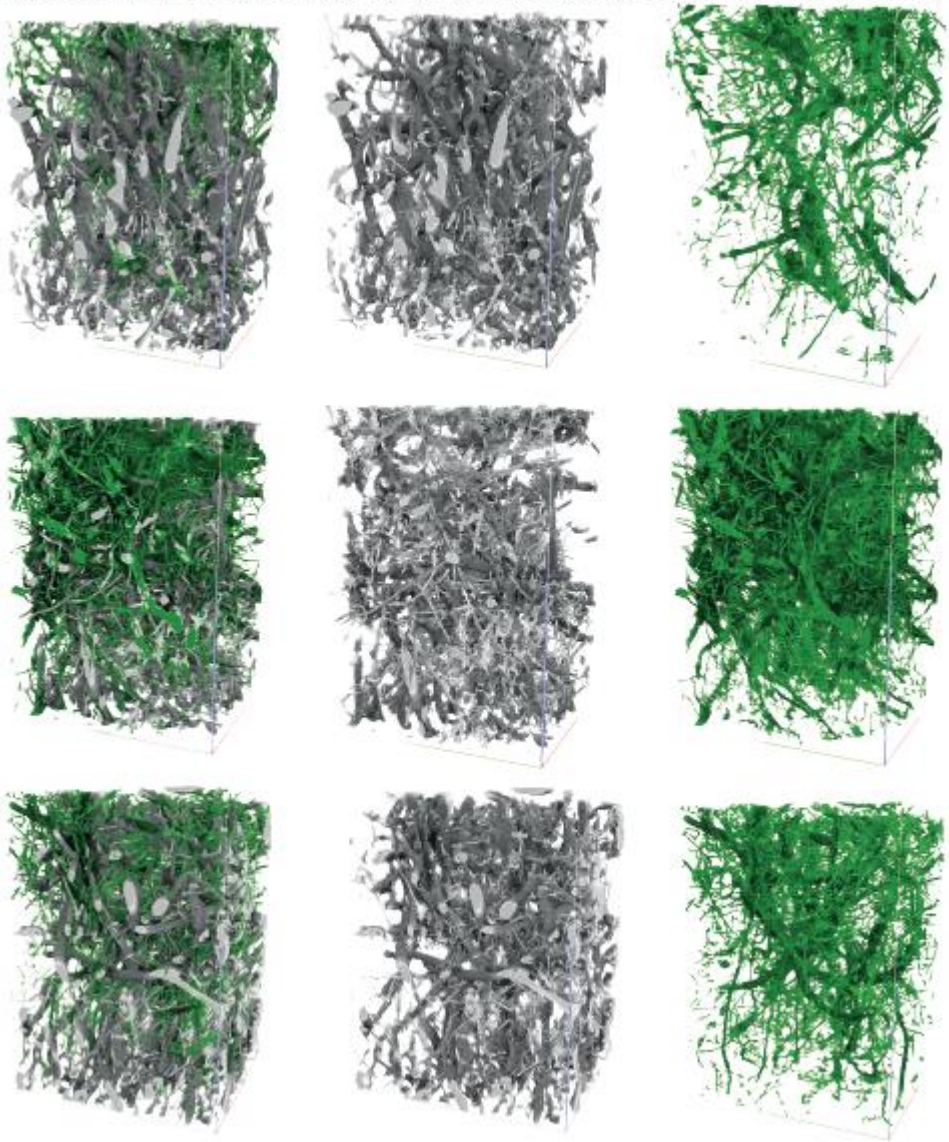

Appendix 1h: Warton Sands, *Spartina spp* (top to bottom: WS SPA1, WS SPA2, WS SPA3)

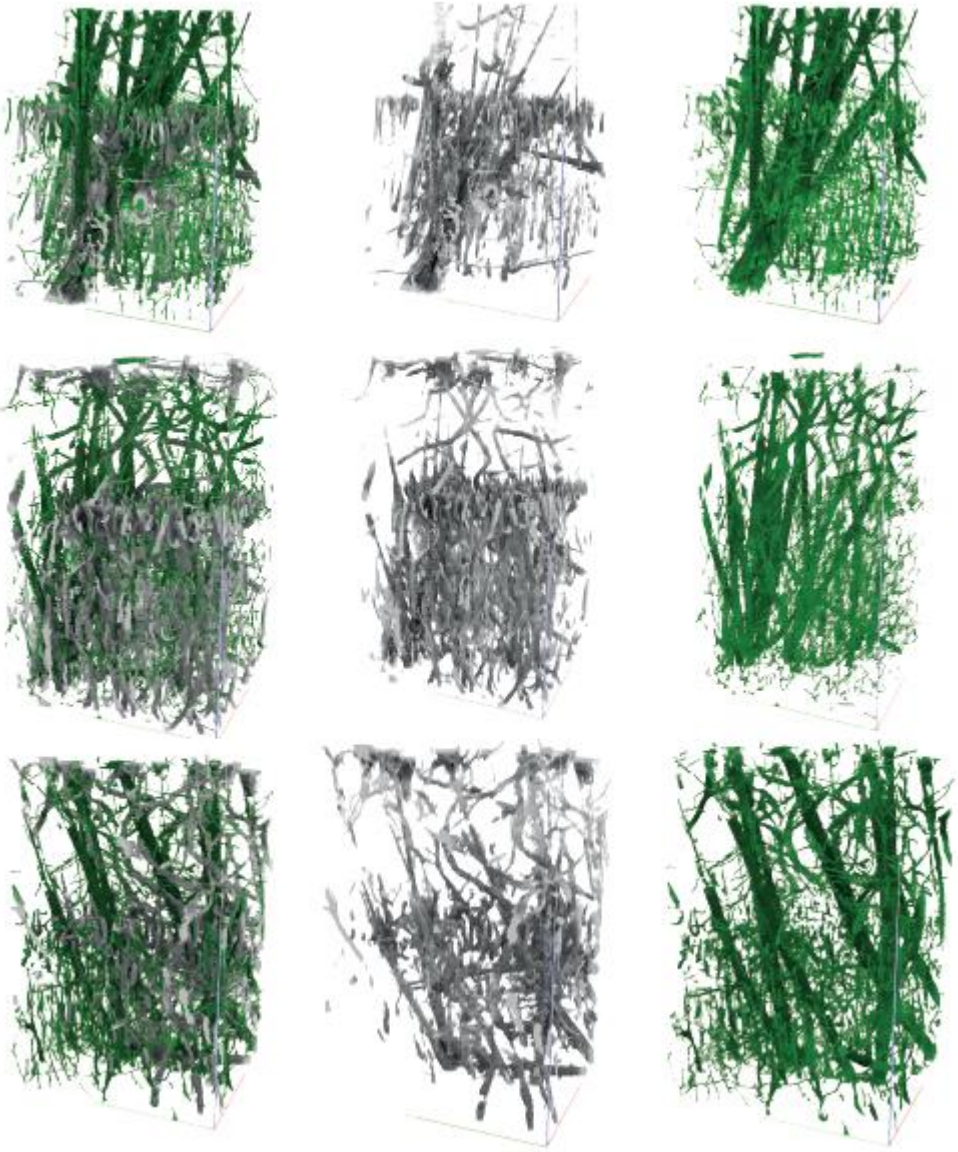

Appendix 1: 3D visualisation of pores and organic matter elements for all 8 stations, showing the differences between replicate cores. Pore features are represented in grey and organic matter elements in green. Left to right: pores + organic matter elements, pores, organic matter elements.

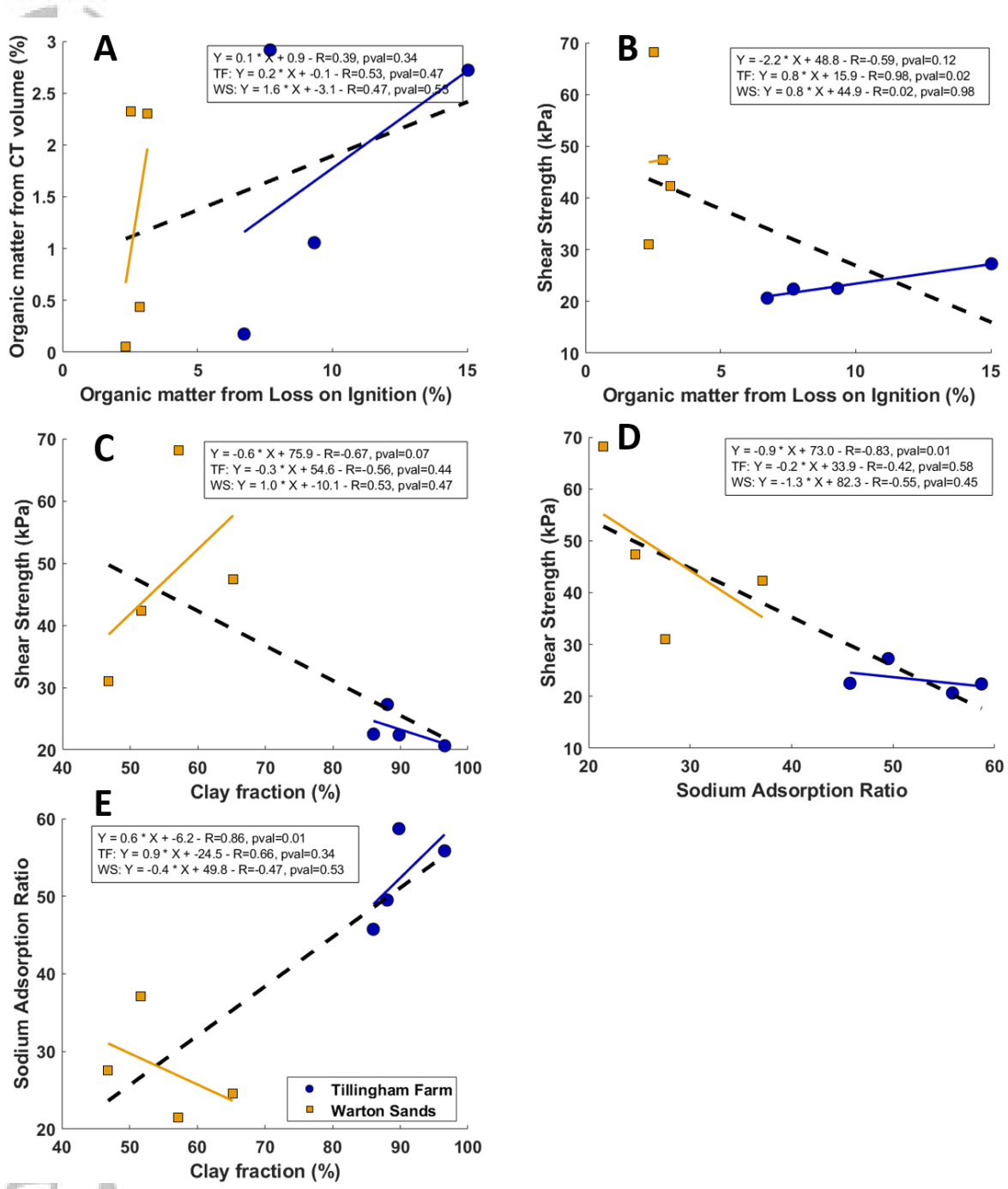

Appendix 2: Visualization of the correlations between geotechnical and sedimentological properties at the two saltmarshes. Linear correlation tests were done over the whole dataset (dashed line) and for each study site (solid lines). Linear correlations were tested between A: organic matter content from loss on ignition and the organic fraction obtained from the µCT data; B: shear strength and organic matter content from loss on ignition; C: shear strength and clay fraction; D: shear strength and sodium adsorption ratio and E: sodium adsorption ratio and clay fraction.

Effect of vegetation cover and sediment type on 3D subsurface structure and shear strength in saltmarshes

Clementine Chirol[1*], Kate L. Spencer[1], Simon J. Carr[2], Iris Möller[3], Ben Evans[4], Jason Lynch[5], Helen Brooks[4], Katherine R Royse[6]